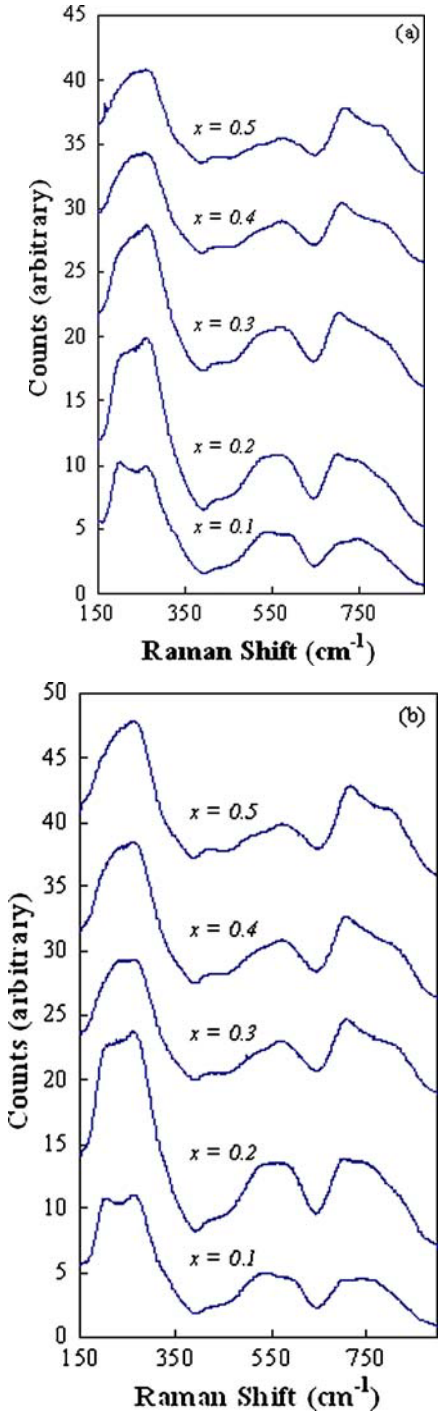

Fig. 9 Raman spectroscopy curves for xPZN–$(1-x)$PZT ceramics prepared by (a) conventional and (b) columbite methods. The ceramics were sintered at 1250°C for $x = 0.1$ and 0.2 and 1225°C for $x = 0.3$–0.5 for 2 hours

method is illustrated in Fig. 11. The coefficient d_{33} increases with increasing sintering temperature up to 1225°C and then decreases for all compositions. It is clearly apparent that the optimum processing condition is sintering at 1225°C for 2 hours. The lower d_{33} values in ceramics sintered at

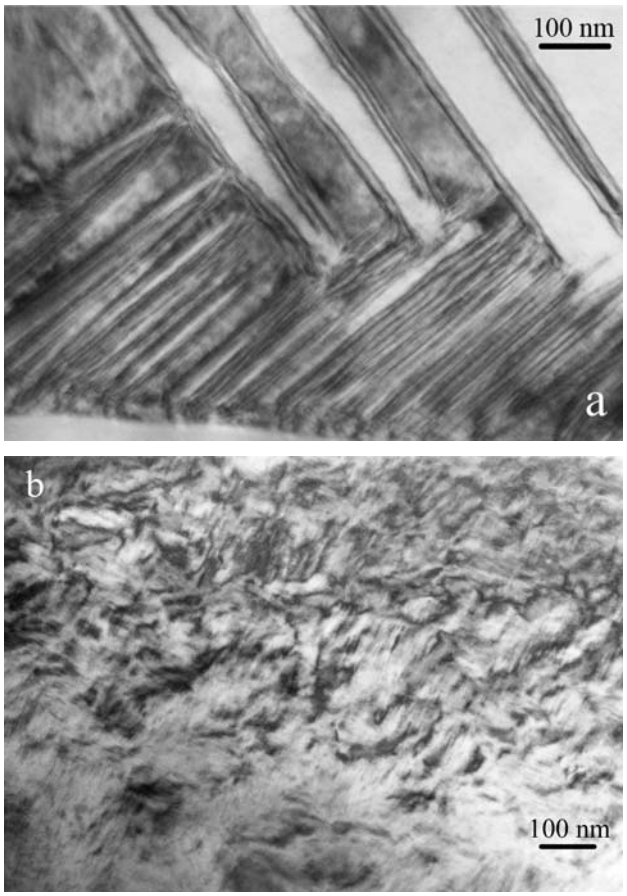

Fig. 10 TEM bright field images of ferroelectric domains in ceramics prepared by the columbite method: (a) 0.1PZN–0.9PZT ceramic sintered at 1250°C for 2 hours; and (b) the 0.5PZN–0.5PZT ceramic sintered at 1225°C for 2 hours

1250°C are presumably due to the PbO loss during the sintering process. Also evident in Fig. 11 is that the composition 0.3PZN–0.7PZT exhibits the highest piezoelectric coefficient d_{33} among all the compositions. It is interesting to note from Fig. 8 that this composition possesses a rhombohedral symmetry at room temperature and is very

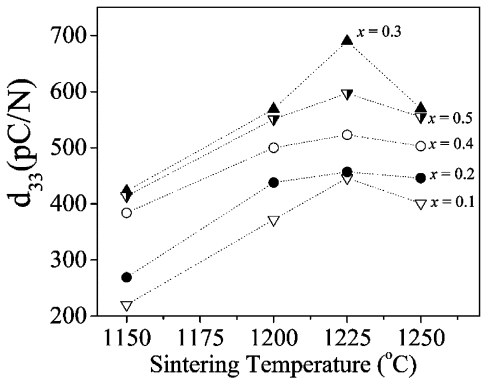

Fig. 11 Piezoelectric coefficient d_{33} as a function of sintering temperature for xPZN-$(1-x)$PZT ceramics prepared via columbite method. The duration for sintering was 2 hours

Table 2 Comparison of the piezoelectric properties observed in this study with previous studies

Ceramics	k_p (%)	d_{33}	References
$Pb(Zr_{0.53}Ti_{0.47})O_3$	52	220	[1]
$0.5PZN–0.5Pb(Zr_{0.47}Ti_{0.53})O_3$	67	430	[12]
$0.5PZN–0.5Pb(Zr_{0.5}Ti_{0.5})O_3$	67	600	Present study
$0.3PZN–0.7Pb(Zr_{0.5}Ti_{0.5})O_3$	70	690	Present study

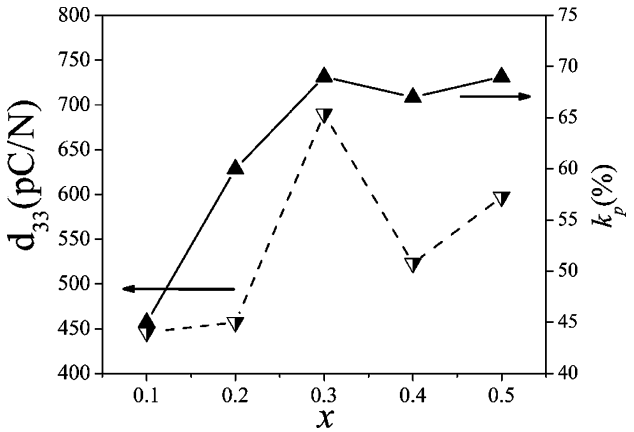

Fig. 12 Piezoelectric properties of d_{33} and k_p in ceramics prepared with the columbite method and sintered at 1250°C for $x = 0.1$–0.2 and 1225°C for $x = 0.3-0.5$ dwell 2 hours

close to the MPB. The observation is consistent with other relaxor-normal ferroelectric solid solution systems, such as the $Pb(Mg_{1/3}Nb_{2/3})$– $PbTiO_3$ and the $Pb(Zn_{1/3}Nb_{2/3})$–$PbTiO_3$ systems, where ultrahigh piezoelectric properties were found in the rhombohedral phase close to the MPB. [3, 8].

The piezoelectric coefficient d_{33} of the ceramics synthesized via the columbite method sintered at optimum conditions is replotted against the composition parameter x in Fig. 12, together with the electromechanical coupling factor k_p. High coupling factor values are noted in compositions of $x = 0.3$, 0.4 and 0.5, among which the composition 0.3PZN–0.7PZT displays the highest values. In Table 2, the piezoelectric properties observed in this study are compared with a previous study where the conventional mixed-oxide method was utilized. It is clear that ceramics with excellent piezoelectric properties can be produced in the xPZN–$(1-x)$PZT pseudo-binary system.

3.5. The PZN–PZT phase diagram

All the above results can be combined into a phase diagram which shows the complete picture of the ferroelectric $Pb(Zn_{1/3}Nb_{2/3})O_3-Pb(Zr_{0.5}Ti_{0.5})O_3$ system (Fig. 13). The data used in this phase diagram were derived from the dielectric measurements on columbite-method prepared ceramics. The two data points at $x = 0.3$ were obtained from the two peaks on the ε_r versus T curve

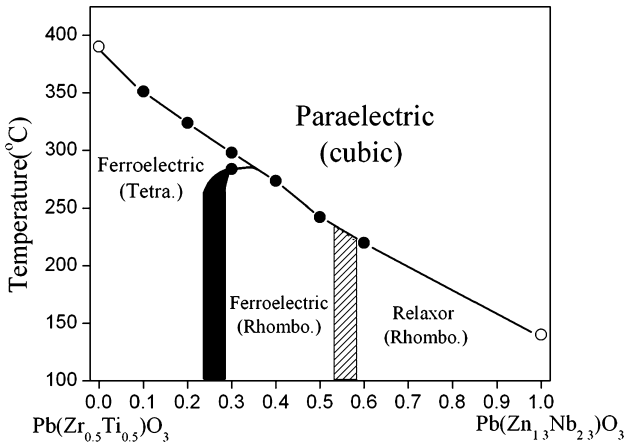

Fig. 13 The proposed phase diagram for the $Pb(Zn_{1/3}Nb_{2/3})O_3-Pb(Zr_{0.5}Ti_{0.5})O_3$ pseudo-binary solid solution system. The solid circles represent data points obtained from the present study, the open circles represent data taken from reference 1

from Fig. 5(a). According to this phase diagram, the $0.3Pb(Zn_{1/3}Nb_{2/3})O_3-0.7Pb(Zr_{0.5}Ti_{0.5})O_3$ ceramic transforms from ferroelectric rhombohedral phase to ferroelectric tetragonal phase at 283.6°C and to a paraelectric cubic phase at 298.8°C. The shaded range between $x = 0.5$ and 0.6 denotes a transition from a normal ferroelectric to a relaxor ferroelectric. As expected, the best piezoelectric properties were observed in the $0.3Pb(Zn_{1/3}Nb_{2/3})O_3-0.7Pb(Zr_{0.5}Ti_{0.5})O_3$ ceramic.

4. Conclusions

Investigations on the structure and properties of the $xPb(Zn_{1/3}Nb_{2/3})O_3-(1-x)Pb(Zr_{0.5}Ti_{0.5})O_3$ system over the range $x = 0.1-0.6$ have revealed an MPB between $x = 0.2$ and 0.3, separating a tetragonal phase from a rhombohedral phase. A normal ferroelectric to relaxor ferroelectric transition is also observed around $x = 0.5$ to 0.6. This transition corresponds to a gradual decrease in the rhombohedral distortion in the structure and a gradual increase in the frequency dispersion of the dielectric response. As expected, excellent piezoelectric properties were obtained for the $0.3Pb(Zn_{1/3}Nb_{2/3})O_3-0.7Pb(Zr_{0.5}Ti_{0.5})O_3$ composition.

Acknowledgments The authors are grateful to the Thailand Research Fund (TRF), Graduate School at Chiang Mai University and King Mongkut's Institute of Technology Ladkrabang for financial support.

References

1. B. Jaffe and W.R. Cook, *Piezoelectric Ceramic* (R.A.N. Publishers, 1971).

2. B. Noheda, D.E. Cox, G. Shirane, R. Guo, B. Jones, and L.E. Cross, *Phys. Rev. B*, **63**, 014103 (2001).
3. B. Noheda, J.A. Gonzalo, L.E. Cross, R. Guo, S.-E. Park, D.E. Cox, and G. Shirane, *Phys. Rev. B*, **61**, 8687 (2000).
4. L. Bellaiche, A. Garcia, and D. Vanderbilt, *Ferroelectrics*, **266**, 41 (2002).
5. V.A. Bokov and I.E. Myl'nikova, *Sov. Phys.-Solid State*, **3**, 631 (1961).
6. J. Kuwata, K. Uchino, and S. Nomura, *Ferroelectrics*, **37**, 579 (1981).
7. V.A. Bokov and I.E. Mylnikova, *Sov. Phys-Solid State*, **2**, 2428 (1960).
8. T.R. Shrout and A. Halliyal, *Am. Ceram. Soc. Bull.*, **66**, 704 (1987).
9. A. Halliyal, U. Kumar, R.E. Newnham, and L.E. Cross, *Am. Ceram. Soc Bull.*, **66**, 671 (1987).
10. J.R. Belsick, A. Halliyal, U. Kumar, and R.E. Newnham, *Am. Ceram. Soc. Bull.*, **66**, 664 (1987).
11. T R. Shrout, Z.P. Chang, N. Kim, and A. Markgraf, *Ferroelectr. Lett.*, **12**, 63 (1990).
12. H. Fan and H.-E. Kim, *J. Appl. Phys.*, **91**, 317 (2002).
13. N. Vittayakorn, G. Rujijanagul, T. Tunkasiri, X. Tan, and D. P. Cann, *Mat. Sci. Eng. B*, **108**, 258 (2004).
14. N. Vittayakorn, G. Rujijanagul, T. Tunkasiri, X. Tan, and D. P. Cann, *J. Mater. Res.*, **18**, 2882 (2003).
15. S.L. Swartz and T.R. Shrout, *Mater. Res. Bull.*, **17**, 1245 (1982).
16. M.-S. Yoon and H.M. Jang, *J. Appl. Phys.*, **77**, 3991 (1995).
17. K. Uchino and S. Nomura, *Ferroelectr. Lett. Sect.*, **44**, 55 (1982).

Appl. Phys. A 83, 295–299 (2006)
DOI: 10.1007/s00339-006-3486-3

Applied Physics A
Materials Science & Processing

S. EITSSAYEAM
U. INTATHA
G. RUJIJANAGUL
K. PENGPAT
T. TUNKASIRI✉

Structural and electrical properties characterization of $(1–x)PbZr_{0.52}Ti_{0.48}O_3–xBaFe_{0.5}Nb_{0.5}O_3$ system

Department of Physics, Faculty of Science, Chiang Mai University, Chiang Mai 50200, Thailand

Received: 18 May 2005/Accepted: 17 December 2005
Published online: 27 January 2006 •

ABSTRACT The structural and electrical properties of $(1-x)PbZr_{0.52}Ti_{0.48}O_3–xBaFe_{0.5}Nb_{0.5}O_3$ ceramics system with the composition near the morphotropic phase boundary were investigated as a function of the $BaFe_{0.5}Nb_{0.5}O_3$ content by X-ray diffraction (XRD) and dielectric measurement technique. Studies were performed on the samples prepared by solid state reaction for $x = 0.1$, 0.2, 0.3, 0.4 and 0.5. The XRD analysis demonstrated that with increasing BFN content in $(1-x)$PZT–xBFN, the structural change occurred from the tetragonal to the cubic phase at room temperature. Changes in the dielectric behavior were then related to these structural depending on the BFN content.

PACS 77.84.Dy; 77.22.Ch; 77.22.Gm

1 Introduction

$Pb(Zr_xTi_{1-x})O_3$ (generally known as PZT) is a solid solution of perovskite ferroelectric $PbTiO_3$ and antiferroelectric $PbZrO_3$. The PZT has been considered as an important material for a wide range of piezoelectrics, pyroelectrics and ferroelectrics device applications such as transducers, memory chip, transformer and pyroelectric sensors [1, 2]. Since the discovery of relaxor behavior in $Pb(Mg_{1/3}Nb_{2/3})O_3$ [3], $Pb(Zn_{1/3}Nb_{2/3})O_3$ [4], $Pb(Ni_{1/3}Nb_{2/3})O_3$ [5] and $Ba(Fe_{0.5}Nb_{0.5})O_3$ [6, 7]. The studies of relaxor ferroelectrics with $AB'_{(1-x)}B''_xO_3$-type perovskite have attracted much attention because of their excellent dielectric and electromechanical properties. $Pb(Zr_{0.52}Ti_{0.48})O_3$ and $Ba(Fe_{0.5}Nb_{0.5})O_3$ belong to the perovskite structural family with general formula ABO_3 (A = mono or divalent ions, B = tri- to pentavalent cations). It is well established that the physical properties or device parameters of PZT can be tailored by synthesizing the materials with improved processing techniques and making suitable substitutions of A and/or B sites. The electrical properties of relaxor ferroelectrics are greatly influenced by the manner in which the B site cations (B′ and B″ ions) are distributed and ordered on the B site sublattice. The Zr/Ti ratio is known to strongly influence properties, such as the elastic constant, the dielectric constant, the coupling factor, etc.

✉ Fax: +66-5335-7512, E-mail: tawee@chiangmai.ac.th

In spite of the evident effect of the BFN on the PZT by solid state reaction, the phase evolution and behavior of electrical properties of dense ceramic bodies of materials obtained by the solid state reaction are not clearly understood. Therefore, we decided to prepare $(1-x)$PZT–xBFN ($x = 0.1$ to 0.5) powders and subjected the sintered to an extensive characterization and microstructure and dielectric properties.

2 Experimental

The PZT–BFN ceramics used in this study are prepared from powders using the conventional mixed-oxide method. The $(1-x)PbZr_{0.52}Ti_{0.48}O_3–xBaFe_{0.5}Nb_{0.5}O_3$ ($1-x$PZT–xBFN) powders were first prepared by mixing the starting materials PbO (> 99%), ZrO_2 (> 99%), TiO_2 (> 99%), $BaCO_3$ (> 99%), Fe_2O_3 (99.9%) and Nb_2O_5 (99.9%) powders in the desired mole ratio, ($x = 0.1$, 0.2, 0.3, 0.4 and 0.5). These powders were ball-milled for 24 h in polyethylene container with zirconia balls. Ethanol was used as a milling medium. After drying at 120 °C, the mixed powders were then calcined at 800–1100 °C for 2 h with heating and cooling rate of 5 °C/min. Subsequently, the most appropriate calcined samples were pressed into disc shape and sintered at various temperatures ranging from 1150 to 1300 °C depending upon the compositions. The samples were heated for 2 h with constant heating and cooling rates of 5 °C/min. The physical characteristics of the ceramics were then determined with the following procedures. The densities of the sintered ceramics were measured by Archimedes method. The phase formations of the calcined powders and sintered specimens were studied by an X-ray diffractometer (Philips model X-pert) at 40 kV and 30 mA in the 2θ range from 10 to 60 degrees with step scan of 0.01°. The microstructure was examined by the scanning electron microscopy (Jeol model 6335F).

For electrical property characterizations, the sintered samples were ground to obtain parallel faces, and the faces were then coated with silver paste as electrodes. The samples were heat-treated at 750 °C for 12 min to ensure the contact between the electrodes and the ceramic surfaces. The dielectric constant and loss tangent of the sintered ceramics were measured as a function of temperature at 1 kHz with an automated dielectric measurement system. The system consists of an LCR-meter (Hioki 3532-50) and a furnace tube, both furnace temperature and dielectric properties were controlled and recorded by a computer. The capacitance and the di-

electric loss tangent were determined over the temperature range of 30 and 400 °C at the frequency 1 kHz. The polarization versus electric field hysteresis loop was measured using a Sawyer–Tower circuit at temperatures between room temperature and 220 °C.

3 Result and discussion

The XRD results of calcined $(1-x)$PZT–xBFN powders showed that the perovskite structure of PZT started to form at 800 °C. It was clearer at higher calcining temperatures and was most pronounced at 1100 °C. No trace of pyrochlore phase was detected. Therefore, the powder calcined at 1100 °C was employed to prepare ceramic samples. After that the $(1-x)$PZT–xBFN ceramics were prepared from optimum condition of calcined powder. The sintering temperature was varied from 1150 to 1300 °C. Figure 1 shows the relationship of density against temperature of the ceramic sample in $(1-x)$PZT–xBFN system $x = 0.1$, 0.2, 0.3, 0.4 and 0.5 or denoted as P9B1, P8B2, P7B3, P6B4 and P5B5 respectively. These results showed that the optimum density depended on sintering temperature. Maximum density of $(1-x)$PZT–xBFN was found at 1250 °C for P9B1 and P8B2, at 1200 °C for P7B3, P6B4 and at 1300 °C for P5B5. These are 7.68, 7.50, 7.30, 7.22 and 7.00 g/cm^3 for P9B1, P8B2, P7B3, P6B4 and P5B5 respectively, comparable to the theoretical value of PZT 8.006 g/cm^3 [8] and according to the inorganic crystal structure database (ICSD) [9], the density of BFN is 6.51 g/cm^3. In the same way, phase evolution of $(1-x)$PZT–xBFN ceramics of each sintered temperature was investigated by XRD techniques. Figure 2 shows the X-ray diffractograms of the highest density ceramics. The results indicated that change of crystal structure occurred as a function of PZT-BFN compositions. Ferroelectric tetragonal PZT phase appeared as $x = 0.1$. Mixed tetragonal and cubic phases began to occur at $x = 0.2$ and completely transforms to paraelectric cubic phase when $x \geq 0.3$, as can be seen at (001) and (100) peaks. Similar result was also found by Vittayakorn et al. [10] who studied the $(1-x)$PZT–xPZN, when $x \geq 0.2$. Neither BFN nor other impurities were detected. The lattice parameters of the two co-existing ferroelectric phases in the ceramics were calculated by the refinement method. The cell parameters and tetragonality (c/a) obtained for each PZT-BFN composition is given in Fig. 3. The result of the cell refinement showed that the $(1-x)$PZT–xBFN system having BFN content in the range $x = 0.3$ and 0.5 has single phase cubic symmetry, with cell parameters dependent on the BFN content. The value of the c/a parameter decreased from 1.02 to 1.00 when the BFN content increased from $x = 0.1$ to 0.3, comparable to that report by Thammajaree et al. [11] who obtains the c/a value of PZT as 1.015 after heating at 1200 °C. At higher x values the parameter (a) of the cubic PZT-BFN phase slightly decreased from 4.043–4.042 Å. These values are comparable to that in the inorganic crystal structure database ICSD No. 43622 $(a = 4.045)$. The X-ray diffraction (XRD) pattern of the BFN ceramic (Fig. 2) shows the single phase of cubic structure. The analysis was carried out based on the ICSD No. 43622 [7]. Even though our result is agreeable to those obtained by Rama et al. [7] and Tezaka et al. [12] who also prepared the samples via solid state reaction, the accurate crystal structure of BFN is still controversial. This is because the structural analysis of BFN ceramic performed by Saha and Sinha [6], using a standard computer program (POWD), gave different results

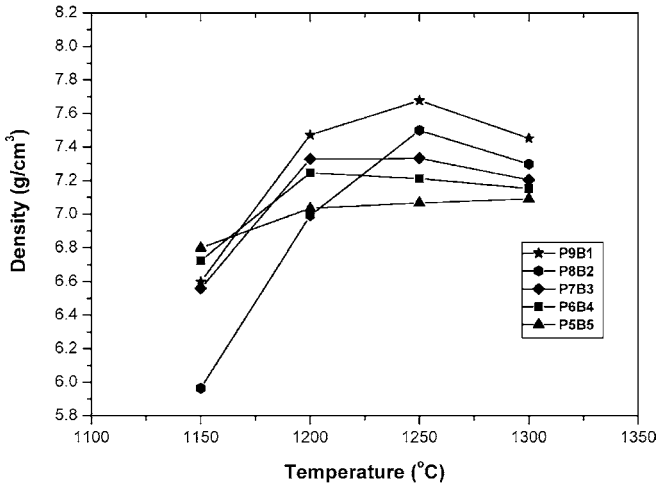

FIGURE 1 Shows the effect of sintering on the density of ceramics

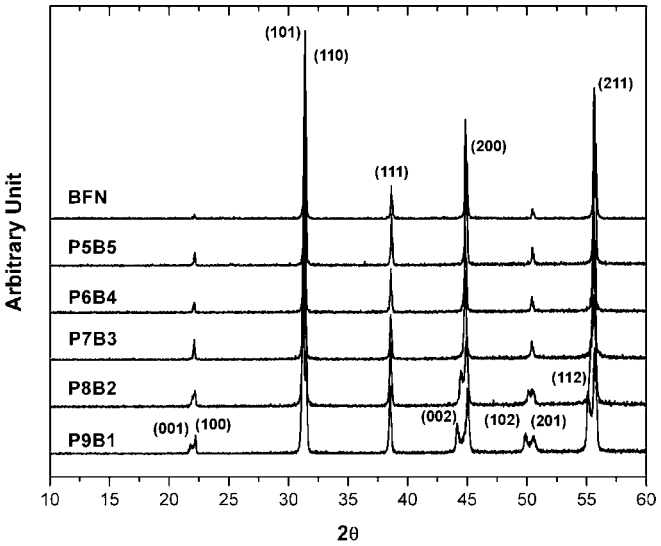

FIGURE 2 X-ray patterns of ceramic at maximize bulk density condition

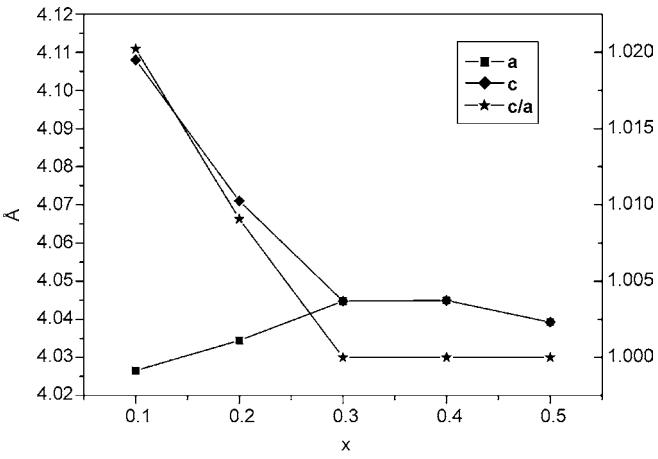

FIGURE 3 Lattices parameter of $(1-x)$PZT–xBFN system

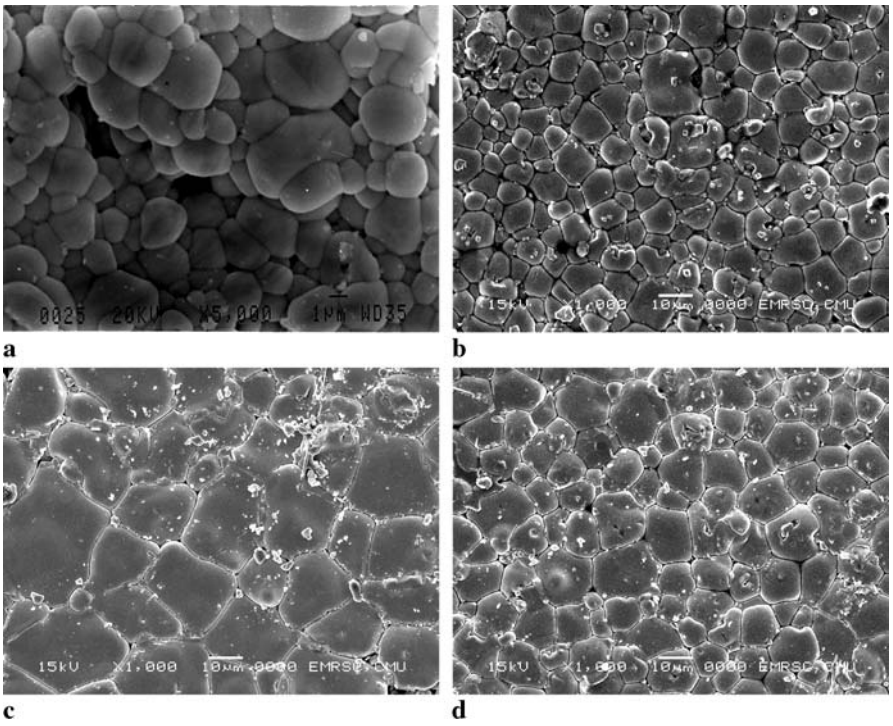

FIGURE 4 SEM micrograph of PZT and $(1-x)$PZT–xBFN ceramics. (**a**) PZT ceramic with average grain size = 1.66 μm, (**b**) P9B1 ceramic with average grain size = 5.03 μm, (**c**) P8B2 ceramic with average grain size = 15.68 μm, (**d**) P7B3 ceramic with average grain size = 8.65 μm

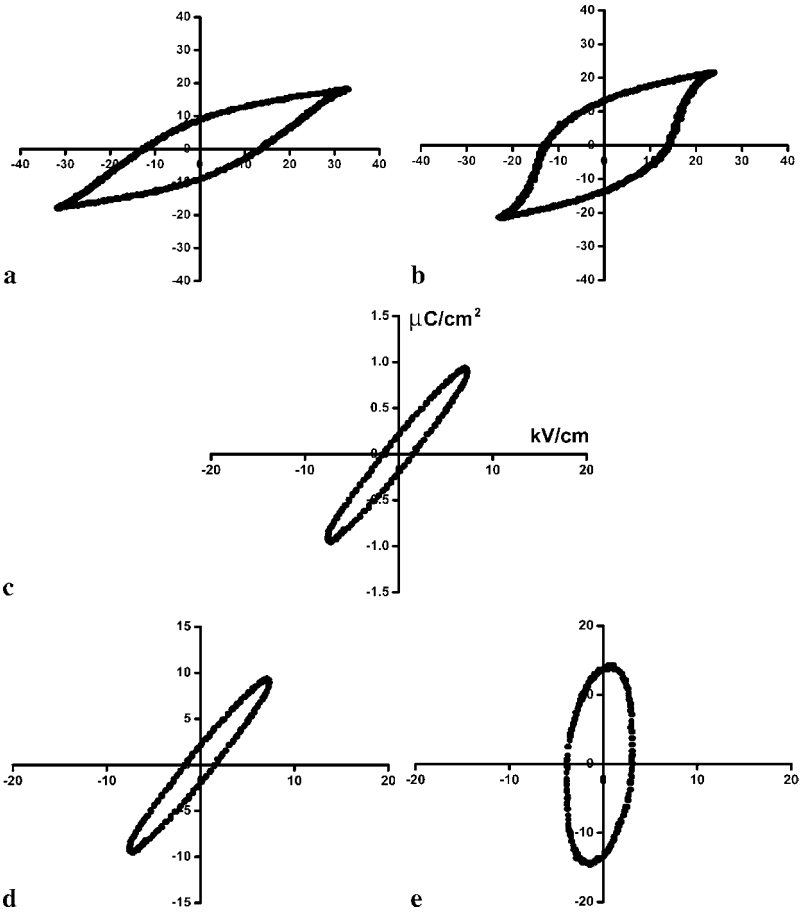

FIGURE 5 Effect of composition (x) on P–E hysteresis loops for $(1-x)$PZT–xBFN system processed at the optimum processing conditions measures at room temperature. (**a**) P9B1, (**b**) P8B2, (**c**) P7B3, (**d**) P6B4 and (**e**) P5B5

from the monoclinic-type structure was evaluated in stead of the cubic one.

The SEM micrographs of the $(1-x)$PZT–xBFN ceramics were compared with that of pure PZT ceramic (Fig. 4). It can be seen that only single phase appeared in all micrographs, and no other phase was observed. The small addition of BFN of about $x = 0.1$ causes significant increase on grain size (Fig. 4b) and reaches maximum of about 15 μm at $x = 0.2$

(Fig. 4c). Then the average grain size is reduced at approximately 8 μm when the BFN content is increased up to 0.3 (Fig. 4d). Over this point, the gradually decrease in grain size is observed. These variations are mainly attributed to the solubility of BFN in the PZT system. The certain solubility value of BFN of about 0.2 is allowed in this system and beyond this solubility limit it is believed to segregate at grain boundaries, resulting in inhibition of grain growth. This is consistent with the work done by Yang et al. [13]. Moreover, the XRD pattern of $(1-x)$PZT–xBFN ceramic at around this solubility limit of $x = 0.2$, contains the mixing of both tetragonal and cubic structures. It may be assumed that the morphotropic phase boundary of the $(1-x)$PZT–xBFN ceramic is near to $x = 0.2$. This can be confirmed by the hysteresis loop measurement of the $(1-x)$PZT–xBFN as shown in Fig. 5. The typical ferroelectric hysteresis loop could only be found in the samples of x up to 0.2, and beyond this morphotropic phase boundary the ellipse loops, indicating lossy linear capacitor.

The relationships between dielectric properties and temperature are shown in Figs. 6 and 7. It was clearly shown that the relative dielectric constant depends on temperature measured at 1 kHz on the ceramic sample of $(1-x)$PZT–xBFN system. In the first set (P9B1, P8B2 and P7B3), the broadness of the dielectric constant peak increased with increasing BFN content. Since the Curie temperature for all of investigated compositions in the first set showed a tendency to decrease from 280 °C to below 30 °C. Not only does the Curie temperature decrease, but also the maximum dielectric constant decreases from 13 350 to 5460 for P9B1 and P7B3 respectively. Considerable broadening of dielectric constant curves was found to increase, with the dielectric loss lower than 0.05 at working temperature (room temperature to 200 °C). On the other hand, the dielectric behaviors of second set materials (P6B4 and P5B5) change in the dielectric peak broadening considerably, while the maximum dielectric constant

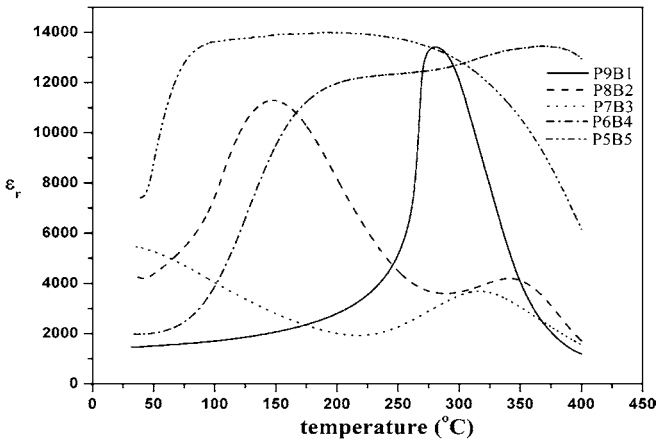

FIGURE 6 The relationship between dielectric permittivity and temperature

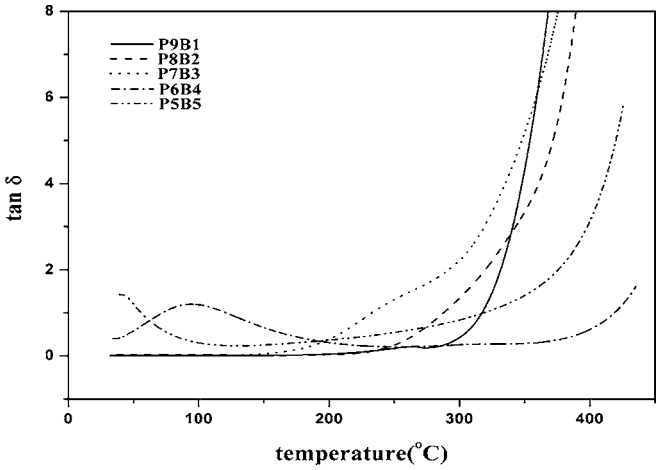

FIGURE 7 The relationship between dielectric loss and temperature

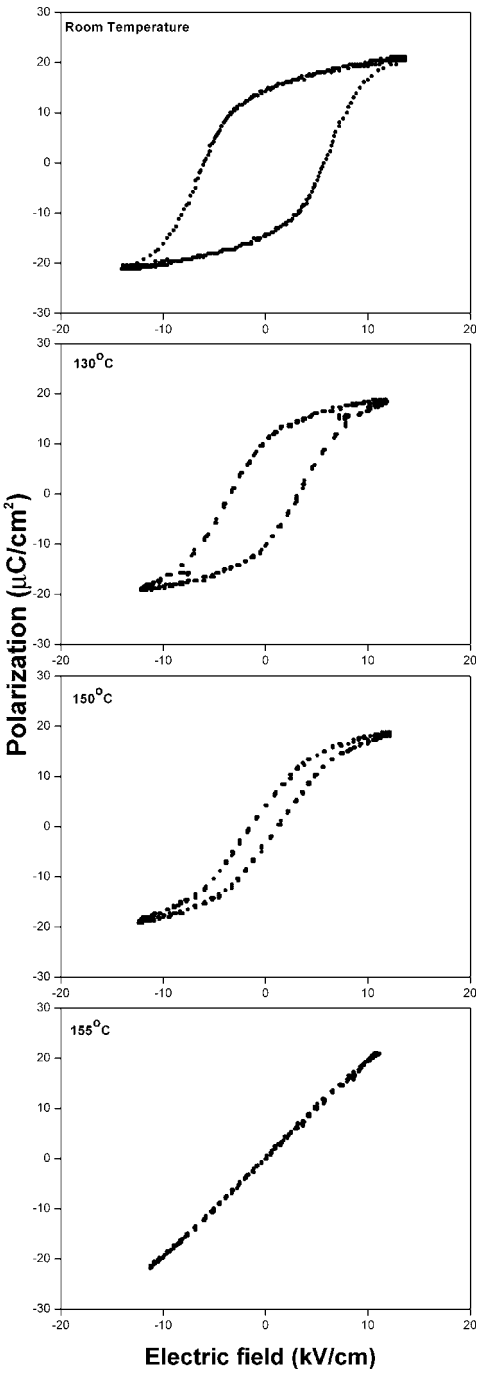

FIGURE 8 Temperature dependence of the P–E hysteresis loops of P8B2 ceramics at the optimum sintering conditions

increased from 12 400 to 14 000 for P6B4 and P5B5 respectively, but with quite high dielectric losses. Furthermore, it was seen that the role of BFN affected the dielectric properties of samples. When BFN content are more than 40 percent per mole the dielectric behavior is close to pure BFN [6].

The hysteresis loops of the P8B2 sample at various temperatures are illustrated in Fig. 8. It can be seen that as the temperature increases the hysteresis loop gets thinner and becomes a single line above the Curie temperature ($\approx 150\,^{\circ}$C) when the material is no longer ferroelectric. This typical hysteresis loop behaviors was revealed elsewhere [14].

4 Conclusions

The effect of BFN on the structure and dielectric of $(1-x)$PZT–xBFN system was investigated for various chemical compositions. The $(1-x)$PZT–xBFN (when $x = 0.1$ to 0.5) ceramics were prepared by the mixed oxide method. Lattice parameters of the tetragonal phase and cubic phase were found to vary with chemical composition. The evolution of the tetragonal phase, (100)/(001) transformed to a single peak (100) which indicating cubic symmetry, while optimum sintering temperature was standing at 1250 °C. They were identified as a single PZT phase material with a perovskite structure having the symmetry from tetragonal to cubic when the ratio of BFN increased. The result shown that the dielectric properties of $(1-x)$PZT–xBFN ceramics can be distinguished into two set. First set (P9B1, P8B2 and P7B3), the broadness of dielectric constant peak increased and Curie temperatures showed a tendency to decrease below 30 °C while the dielectric loss was still less than 0.05. On the another hand, second set (P6B4 and P5B5) is large broad peak and high dielectric constant. The SEM micrographs also revealed single phase of the materials.

ACKNOWLEDGEMENTS The authors would like to express their sincere thanks to the Thailand Research Fund, the Royal Golden Jubilee Ph.D. Program, Ministry of University Affairs and Graduate School, Chiang Mai University for financial support throughout the project.

REFERENCES

1 V. Koval, C. Alemany, J. Briancin, H. Brunckova, J. Electroceram. **10**, 19 (2003)
2 G.H. Haertling, J. Am. Ceram. Soc. **82**, 797 (1999)
3 L.E. Cross, Mater. Chem. Phys. **43**, 108 (1996)
4 A. Mergen, W.E. Lee, J. Eur. Ceram. Soc. **17**, 1033 (1997)
5 D.K. Agrawal, A. Halliyal, J. Belsick, Mater. Res. Bull. **23**, 159 (1988)
6 S. Saha, T.P. Sinha, J. Phys.: Condens. Matter. **14**, 249 (2002)
7 N. Rama, J.B. Philipp, M. Opel, K. Chandrasekaran, V. Sankaranarayanan, R. Gross, M.S.R. Rao, J. Appl. Phys. **95**, 7528 (2004)
8 Powder diffraction file. Joint committee on Powder Diffraction Standards (International Center for Diffraction Data Swarthmore, P.A. 1997) No. 33-784
9 The inorganic crystal structure database (ICSD) No. 43622
10 N. Vittayakorn, G. Rujijanagul, T. Tunkasiri, X. Tan, D. Cann, Mater. Sci. Eng. B **108**, 258 (2004)
11 W. Thamjaree, W. Nhuapeng, T. Tunkasiri, Ferroelectric Lett. **31**, 79 (2004)
12 K. Tezuka, K. Henmi, Y. Hinatsu, J. Solid State Chem. **154**, 591 (2000)
13 Z. Yang, X. Zong, H. Li, Y. Chang, Mater. Lett. **59**, 3476 (2005)
14 D.W. Richerson, *Modern Ceramic Engneering*. 2nd edn. (Marcel Dekker, New York 1992)

Available online at www.sciencedirect.com
SCIENCE DIRECT®
Current Applied Physics 6 (2006) 303–306
Current Applied Physics
An official journal of the KPS
www.elsevier.com/locate/cap
www.kps.or.kr

Piezoelectric properties of $(1-x)Pb(Zr_{1/2}Ti_{1/2})O_3$–$xPb(Zn_{1/3}Nb_{2/3})O_3$ ceramics prepared by the columbite–(wolframite) precursor method

N. Vittayakorn [a,*], C. Puchmark [b], G. Rujijanagul [c], X. Tan [d], D.P. Cann [d]

[a] Department of Chemistry, Faculty of Science, King Mongkut's Institute of Technology Ladkrabung, Bangkok 10520, Thailand
[b] Department of Physics, Faculty of Science, Naresuan University, Phitsanulok 65000, Thailand
[c] Department of Physics, Faculty of Science, Chiang Mai University, Chiang Mai 50200, Thailand
[d] Materials Science and Engineering Department, Iowa State University, Ames, IA 50011, USA

Available online 22 December 2005

Abstract

Solid solutions of the perovskite structure, $(1-x)Pb(Zr_{1/2}Ti_{1/2})O_3$–$xPb(Zn_{1/3}Nb_{2/3})O_3$ with $x = 0.1$–0.5, were synthesized via the columbite–(wolframite) precursor method. The phase development of calcined powder precursors was analyzed by X-ray diffraction. Phase-pure perovskite of PZN–PZT ceramics was obtained over a wide compositional range. The microstructure and piezoelectric properties were characterrized by means of scanning electron microscopy (SEM), d_{33} measurements and impedance analysis. It has been found that ultra-high piezoelectric properties were observed in compositions close to a morphotropic phase boundary (MPB). The maximum value of d_{33} (690 pC/N) and the highest k_p (0.7) were recorded for the composition $x = 0.3$ located at the boundary between tetragonal and rhombohedral ferroelectric phases. Furthermore, large values of d_{33} (600 pC/N) and k_p (0.67) were observed at a compositions of $x = 0.5$, which is the boundary between two ferroelectric rhombohedral phases.

PACS: 77.84.Dy; 77.65.–j; 77.80.Bh

Keywords: PZT; Piezoelectricity; Ferroelectricity; Phase transitions

1. Introduction

Lead zinc niobate, $Pb(Zn_{1/3}Nb_{2/3}O_3)$(PZN) is a ferroelectric material with a rhombohedral structure. It shows frequency dependent dielectric relaxation behavior, as well as diffuse phase transition at 140 °C [1,2]. PZN is one of the most important ferroelectric materials. A single crystal of PZN shows extremely high dielectric and piezoelectric constants; much larger than other normal ferroelectric materials such as PZT [3]. However, phase-pure perovskite of PZN is very difficult to synthesize by normal solid-state sintering method due to the PZN, which has low tolerance and a small electronegativity difference between the cations [4].

It is well known that $Pb(Zr_{1-x}Ti_x)O_3$ (PZT) is the most popular ferroelectric material that is used for electronic devices, since PZT shows high piezoelectric properties, with a composition close to a morphotropic phase boundary (MPB) (Zr:Ti 52:48), the boundary between the tetragonal and the rhombohedral phases. In addition, PZT forms solid-solutions easily from the conventional synthesis method.

Since both PZT and PZN have the perovskite structure and are known to have excellent ferroelectric and piezoelectric properties, it is proposed to alloy PZN with PZT to stabilize and optimize the PZN ceramics. Ultra-high piezoelectric properties were expected in this system. Recently, Fan and Kim [5] successfully stabilized perovkite PZN by adding lead zirconate titanate $Pb(Zr_{0.47}Ti_{0.53})O_3$ (PZT) in the process of conventional solid-state reaction. In the present work, the columbite–(wolframite) precursor

* Corresponding author. Tel.: +66 9 700 2136; fax: +66 2 326 4415.
E-mail address: naratipcmu@yahoo.com (N. Vittayakorn).

1567-1739/$ - see front matter © 2005 Elsevier B.V. All rights reserved.
doi:10.1016/j.cap.2005.11.005

method [7] was used to synthesize the $(1-x)$PZT–xPZN; $x = 0.1$–0.5 ceramics. The columbite structure, $ZnNb_2O_6$, and the wolframite structure, $ZrTiO_4$, were selected as the precursors. Piezoelectric properties of the $(1-x)$PZT–xPZN ceramics obtained from the columbite–(wolframite) precursor method were studied.

2. Experimental procedure

Reagent-grade oxide PbO, ZnO, Nb_2O_5 and TiO_2 (anatase-structure) were used as raw materials. The columbite $ZnNb_2O_6$ and wolframite $ZrTiO_4$ precursors were measured and introduced into the batch calculations. After weighing, the mixture was homogenised by ball milling in ethanol with zirconia medium for 24 h. After drying and sieving, the powders were calcined. The reaction between ZnO and Nb_2O_5 was performed at calcination temperatures ranging from 975 to 1125 °C and the $ZrTiO_4$ phase was formed at calcination temperatures ranging from 1000 to 1400 °C. In the present work, the $(1-x)$PZT–xPZN with $x = 0$–0.5 compositions were prepared from $ZrTiO_4$, $ZnNb_2O_6$, and PbO powders. The powders were mixed by ball milling in ethanol for 24 h. After drying, the product was calcined in a double alumina crucible at temperatures between 750 and 950 °C. A constant PbO excess of 2.0 mol% was added to compensate for lead losses during calcination and sintering [6]. The calcined powders were pressed into discs at a pressure of 150 MPa using 0.5 wt.% aqueous solution of poly(vinyl alcohol) as a binder. The pellets were sintered at 1200–1275 °C for 2 h. In order to minimize the loss of lead due to vaporization, the PbO atmosphere for the sintering was maintained using $PbZrO_3$ as a spacer powder. The phase structure of the powders was analyzed by a X-ray diffractometer using CuK_α radiation. The percentage of perovskite phase was estimated from the X-ray peak intensities using the method of Swartz and Shrout [7]. The microstructures of the sintered samples were examined using a scanning electron microscopy (SEM) (JSM5410, JEOL). In order to study the piezoelectric properties, the sintered disks were ground and sputtered with gold on both sides of the samples. The samples were poled in a silicone oil bath at 150 °C for 20 min. The piezoelectric coefficient (d_{33}) was measured by a d_{33} meter (Model 8000 d_{33} Tester). The electromechanical coupling factor (k_p) was established by resonance and anti-resonance frequency using an impedance analyzer (HP 4194A Impedance Analyzer).

3. Results and discussions

Fig. 1 shows XRD patterns of $ZrTiO_4$ powders at varying calcination temperatures. Sharp peaks of crystalline ZrO_2 and anatase-TiO_2 were detected at calcination temperature below 1150 °C. The phase analysis of ZrO_2, rutile-TiO_2, anatase-TiO_2 and $ZrTiO_4$ was carried out using Standard ICDD data. With increasing calcination temperature up to 1150 °C, the results showed that

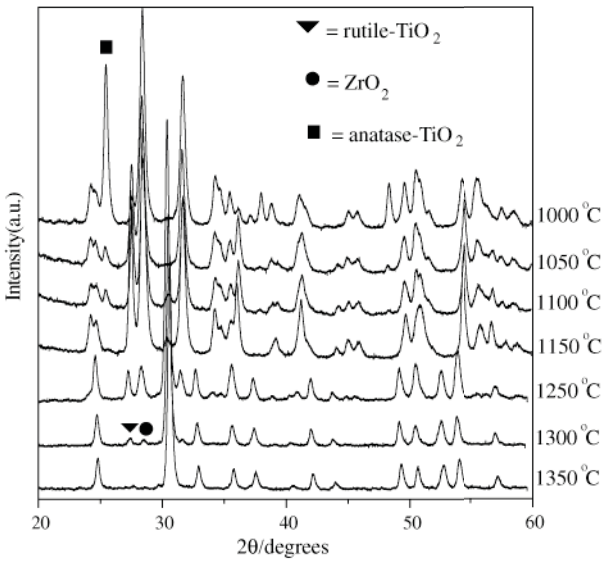

Fig. 1. X-ray diffraction patterns of $ZrTiO_4$ powders at various calcination temperatures.

anatase-TiO_2 changed structure to rutile-TiO_2, which was reported earlier by Navrotsky [8]. The yield of $ZrTiO_4$ phase increased significantly until 1350 °C, when a single phase of $ZrTiO_4$ was formed, revealing that rutile-TiO_2 had completely reacted with the ZrO_2 phase. This major phase, which could be matched with ICDD file no. 34-415, possesses an orthorhombic, space group *Pnab*(no. 60), with the lattice parameter, $a = 5.03$ Å, $b = 5.49$ Å $c = 4.80$ Å. XRD patterns of $ZnNb_2O_6$ powders at varying calcination temperatures are shown in Fig. 2. All samples showed the pure phase of $ZnNb_2O_6$, with no evidence of starting materials ZnO and Nb_2O_5. Moreover, orthorhombic $Zn_2Nb_{34}O_{87}$ and monoclinic $Zn_3Nb_2O_8$ were not detected [11,12]. The XRD patterns of $ZnNb_2O_6$ powders

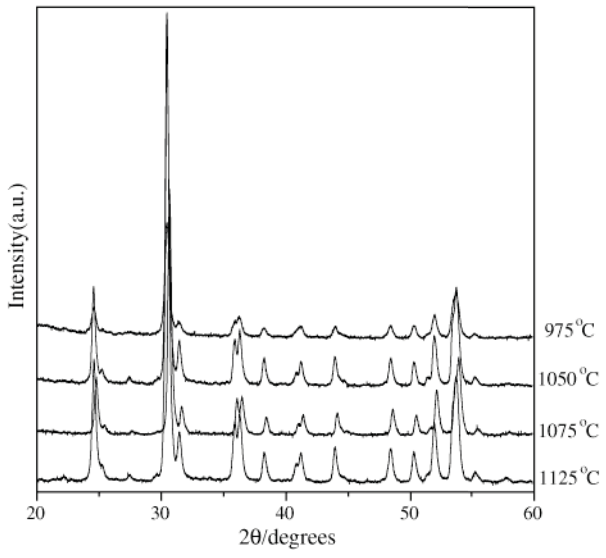

Fig. 2. X-ray diffraction patterns of $ZnNb_2O_6$ powders at various calcination temperatures.

are close to those given in the ICDD file no. 76-1827. This major phase has orthorhombic columbite-type structure with the lattice parameters, $a = 14.20$ Å, $b = 5.726$ Å and $c = 5.04$ Å. In order to prepare PZT–PZN by the columbite–(wolframite) precursor method, the calcination temperatures of 1350 and 975 °C were chosen for wolframite $ZrTiO_4$ and columbite $ZnNb_2O_6$, respectively. $ZrTiO_4$ and $ZnNb_2O_6$, from these chosen conditions were mixed and then calcined at temperatures between 750 and 900 °C. Pyrochlore and impurity phases were formed at temperatures below 900 °C. The effect of calcination temperature on the amount of perovskite for the compositions $x = 0$–0.5 was also studied. The percentage of perovskite phase of all compositions was calculated from the XRD data and is given in Table 1. Generally, the perovskite phase increased with increasing calcination temperature. Phase-pure perovskite was found at 900 °C in all compositions. Thus, the calcination temperature of 900 °C for the columbite method was a suitable temperature for preparing PZT–PZN. All compositions show pure phase perovskite after the sintering process (Fig. 3). Fan and Kim [5] observed phase-pure perovskite of PZT–PZN prepared by the conventional method at calcination temperature of 850 °C. This indicated that the columbite–(wolframite) method requires higher calcination temperatures to eliminate the pyrochlore phase formation than the conventional method. The sintered pellets appeared to be dense, as indicated by the grain packing and a few pores at the triple grain junction. Uniform grains were observed with the average grain size in the range of 1–5 μm, as shown in Fig. 4. It should be noted that no evidence of a rectangular shape of $Pb_3Nb_4O_{13}$ or octahedral shape of $Pb_{1.83}Zn_{0.29}Nb_{1.77}O_{6.39}$ has been reported inside or on the surface of ceramics by other workers [5]. The effect of sintering temperature on the piezoelectric coefficient (d_{33}) of PZT–PZN ceramics prepared via the columbite method is illustrated in Fig. 5. The piezoelectric coefficient (d_{33}) values increased with increasing the sintering temperature up to 1225 °C and then decreased for all compositions. In this work, the d_{33} and k_p experiments showed that the optimum sintering temperature condition for this system was 1225 °C for 2 h. The lower d_{33} values in ceramics sintered at 1250 °C are presumably on account of the PbO loss during the sintering process. The d_{33} and electromechanical coupling factor (k_p) versus PZN composition are illustrated in Fig. 6. In this present work, ultra-high piezoelectric properties were observed in compositions close to MPB. The maximum value of d_{33} (690 pC/N) and the highest k_p (0.7) were recorded for the composition $x = 0.3$ located at the boundary between tetragonal and rhombohedral ferroelectric phases. Furthermore, large values of d_{33}(600 pC/N) and k_p(0.67) were observed at a composition of $x = 0.5$, which is the boundary between two ferroelectric rhombohedral phases. The observation is consistent with other relaxor–normal ferroelectric solid solution systems, such

Table 1
Percentage of perovskite phase of $(1 - x)$PZT–xPZN; $x = 0.1$–0.5

Calcined temperature (°C)	Percentage of perovskite phase				
	$x = 0.1$	$x = 0.2$	$x = 0.3$	$x = 0.4$	$x = 0.5$
700	23.4	–	–	–	–
750	91.3	83.3	30.9	54.5	–
800	98.6	89.6	70.2	58.6	46.7
850	100	91.3	84.0	81.0	76.7
900	100	100	100	100	100
950	100	100	100	100	100

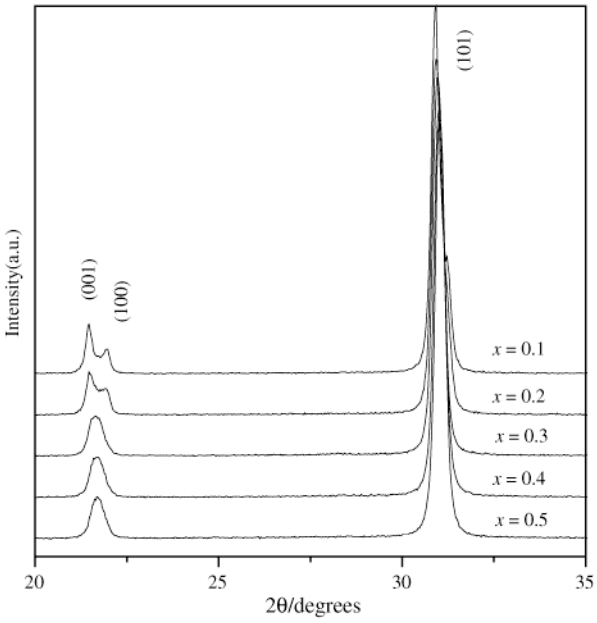

Fig. 3. X-ray diffraction patterns of a sintered $(1 - x)$PZT–xPZN ceramics.

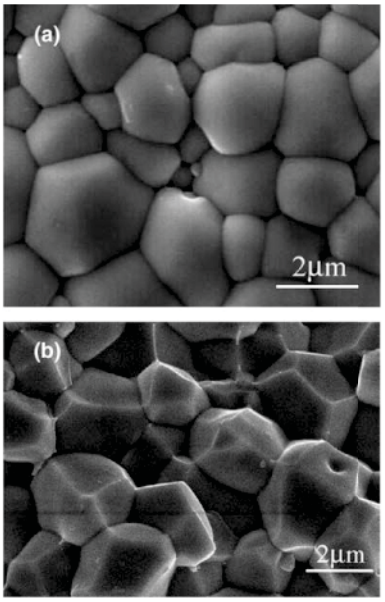

Fig. 4. SEM micrographs of (a) surface and (b) fracture of 0.7PZT–0.3PZN ceramics sintered at 1225 °C.

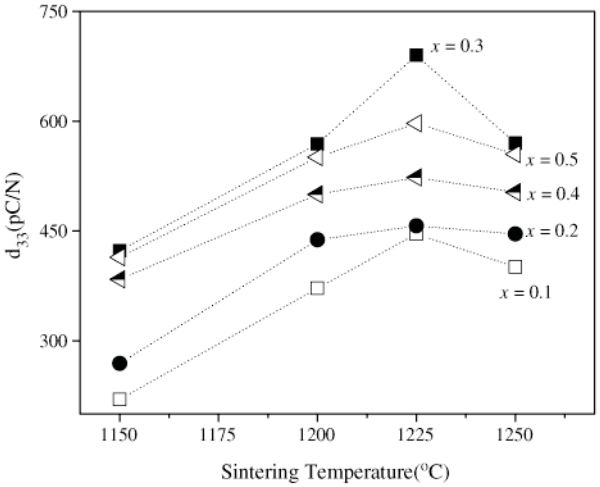

Fig. 5. Piezoelectric coefficient, d_{33} as a function of sintering of perovskite $(1-x)$PZT–xPZN ceramics.

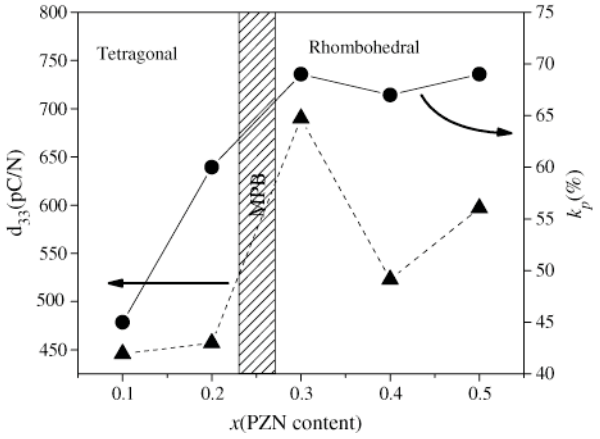

Fig. 6. Piezoelectric coefficient, d_{33} and electromechanical coupling factor, k_p as a function of sintering in $(1-x)$PZT–xPZN ceramics.

as the $Pb(Mg_{1/3}Nb_{2/3})$–$PbTiO_3$ and the $Pb(Zn_{1/3}Nb_{2/3})$–$PbTiO_3$, where ultra-high piezoelectric properties were found in the rhombohedral phase close to the MPB.

Recent literature reviews [5,9] show that there are 2 MPBs in the PZT–PZN system; first, the separated tetragonal phase with rhombohedra phase at the composition 0.75PZT–0.25PZN and the second MPB showing transformation relaxor rhombohedral ferroelectric to normal rhombohedral ferroelectric at the composition 0.5PZT–0.5PZN [9]. It is interesting to note that the PZT–PZN binary system gives ultra-high piezoelectric properties in the composition close to the MPBs. Furthermore, these properties may be improved by heat treatment, which is observed in many relaxor ferroelectric materials [10]. The comparison with ceramic that is prepared by the conventional method, the d_{33} obtained from the columbite method is higher than that obtained from the conventional method. This might be the influence of b-site ordering in the perovskite structure.

4. Conclusions

Columbite ($ZnNb_2O_6$) and wolframite ($ZrTiO_4$) precursors were utilized to prepare highly pure PZN–PZT solid solutions. Superior piezoelectric properties were obtained in the compositions located close to the two MPBs found in this system. The maximum value of d_{33} (690 pC/N) and the highest k_p (0.7) were recorded for the composition $x = 0.3$. Furthermore, high values of d_{33} (600 pC/N) and k_p (0.67) were also observed at composition of $x = 0.5$.

Acknowledgments

The authors are grateful to the Thailand Research Fund, Graduate School at Chiang Mai, Faculty of Science Chiang Mai University and Ministry of University Affairs in Thailand for their financial support.

References

[1] V.A. Bokov, I.E. Mylnikova, Sov. Phys-Solid State 2 (1960) 2428.
[2] K. Uchino, S. Nomura, Ferroelectr. Lett. Sect. 44 (1982) 55.
[3] K. Uchino, Solid State Ionics 108 (1998) 43.
[4] T.R. Shrout, A. Halliyal, Am. Ceram. Soc. Bull. 66 (1987) 704.
[5] H. Fan, H.-E. Kim, J. Appl. Phys. 91 (2002) 317.
[6] N. Vittayakorn, G. Rujijanagul, T. Tunkasiri, X. Tan, D.P. Cann, J. Mater. Res. 18 (2003) 2882.
[7] S.L. Swartz, T.R. Shrout, Mater. Res. Bull. 17 (1982) 1245.
[8] A. Navrotsky, O.J. Kleppa, J. Am. Ceram. Soc. 50 (1967) 626.
[9] N. Vittayakorn, G. Rujijanagul, T. Tunkasiri, X. Tan, D.P. Cann, Mater. Sci. Eng. B 108 (2004) 258.
[10] H. Fan, H.-E. Kim, J. Mater. Res. 17 (2002) 180.
[11] R. Norin, B. Dahlen, Acta. Chem. Scand. 23 (5) (1969) 1836.
[12] R.W. Harrison, E.J. Delgrosso, J. Electrochem. Soc. 110 (3) (1965) 119.

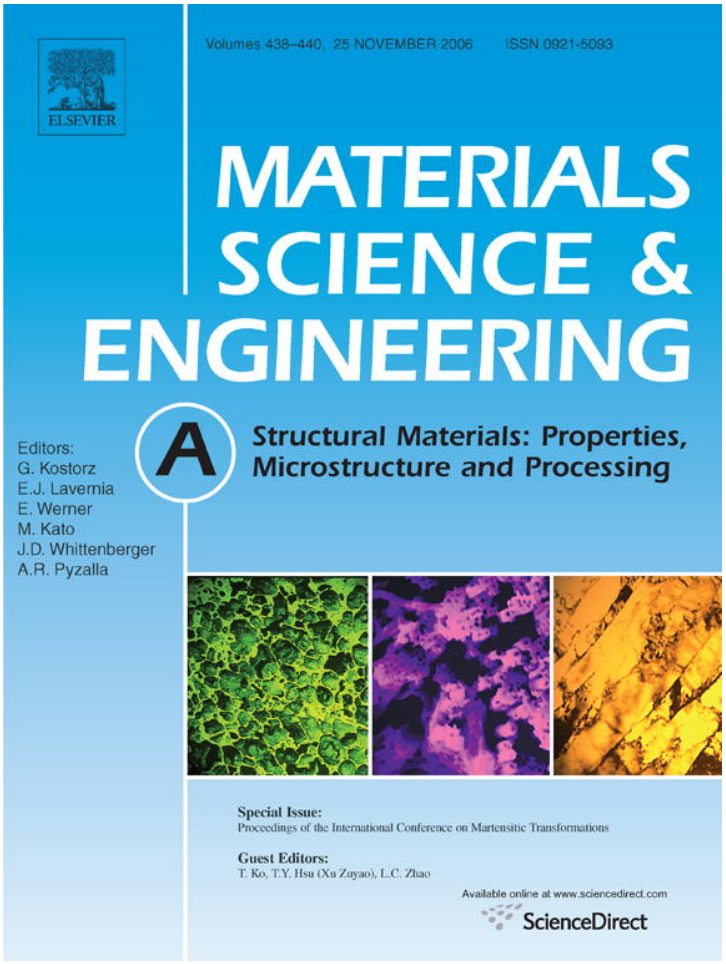

ELSEVIER

Materials Science and Engineering A 438–440 (2006) 360–363

MATERIALS SCIENCE & ENGINEERING A

www.elsevier.com/locate/msea

Phase formation, piezoelectric, dielectric and mechanical properties of $(Pb_{1-x}Ba_x)ZrO_3$ ceramics

G. Rujijanagul [a,*], A. Rittidech [b], T. Bongkarn [c]

[a] *Department of Physics, Faculty of Science, Chiang Mai University, Chiang Mai 50200, Thailand*
[b] *Department of Physics, Faculty of Science, Mahasarakham University, Mahasarakham 44150, Thailand*
[c] *Department of Physics, Faculty of Science, Naresuan University, Pitsanulok 65000, Thailand*

Received 25 April 2005; received in revised form 13 October 2005; accepted 20 December 2005

Abstract

$(Pb_{1-x}Ba_x)ZrO_3$ ceramics for the composition range $0.0 \leq x \leq 0.3$ were prepared by mixed oxide solid-state reaction method. Phase formation, microstructure, piezoelectric, dielectric and mechanical properties were studies. It was found that the density of the ceramics decreases with increasing amounts of Ba^{2+}, whilst the average grain size is in the range of 1.0–2.3 μm. The structure of as-calcined powder revealed that, the fraction of the orthorhombic phase is decreasing with increasing Ba^{2+} content. The mechanical properties of the ceramics were studied by Vickers and Knoop microhardness testers. The values of Vickers and Knoop hardness are in the range of 4.10–6.48 and 4.15–5.67 GPa respectively. The d_{33} values of the samples increases from ~0 to 87 pC/N with increasing Ba^{2+} concentration from $x = 0.0$–0.3. The dielectric constant at room temperature increases with increasing of Ba^{2+} concentration. The results indicated that Ba^{2+} concentration has a significant effect on the electrical properties in PBZ ceramics.

Keywords: $(Pb_{1-x}Ba_x)ZrO_3$; Phase formation; Piezoelectric; Mechanical properties

1. Introduction

Lead zirconate, $PbZrO_3$ (PZ), is one end member of the industrially interesting solid-solution series $PbZrO_3$–$PbTiO_3$ [1] and the first antiferroelectric identified by Sawaguchi et al. [2,3]. At room temperature PZ is an antiferroelectric phase (AFE) which has an orthorhombic structure [2]. It changes from the AFE to a paraelectric phase (PE) and transforms from the orthorhombic structure to the cubic structure at 236 °C [4]. It is reported that there exists a ferroelectric phase (FE) over a very narrow temperature range (230–233 °C) [5–8]. The intermediate FE can also be introduced by partial replacement of Pb^{2+} ions by Ba^{2+} ions. The temperature range of this intermediate phase also increases with the Ba concentration [9–16]. The AFE-FE transition produces a large volume expansion. It makes this material potentially useful for high-displacement electromechanical actuator applications [15,16].

$(Pb_{1-x}Ba_x)ZrO_3$ (PBZ) was discovered by Roberts in 1950 [4]. Later on, many authors prepared and investigated the properties such as structural, dielectric properties, field induced strain behavior and phase transition of PBZ [9–22]. Although the microstructure and mechanical properties of PBZ ceramics are particularly important in the design of displacement electromechanical actuator, they have received much less attention than other active properties. Moreover, the piezoelectric properties of PBZ system have not been clearly understood. Therefore, in this present work, $(Pb_{1-x}Ba_x)ZrO_3$ (PBZ) for $0.00 \leq x \leq 0.30$ were prepared by solid state reaction method. Structural phase formation, densification, microstructure, mechanical, dielectric and piezoelectric properties of PBZ ceramics are investigated as a function of compositions x. The results were discussed and compared with previous data.

2. Experimental procedure

The $(Pb_{1-x}Ba_x)ZrO_3$, $0.000 \leq x \leq 0.300$, powders were prepared by a conventional mixed oxide method. The raw materials of PbO, ZrO_2 and $BaCO_3$ were weighed and mixed by ball-milling in acetone using zirconia ball for 24 h. After drying and seiving, it was calcined at 1000 °C for 1 h. The calcined powders were reground by ball-milling with 1 wt.% binder (B-5

* Corresponding author. Tel.: +66 53 943 376; fax: +66 53 357 512.
E-mail address: rujijanagul@yahoo.com (G. Rujijanagul).

0921-5093/$ – see front matter © 2006 Elsevier B.V. All rights reserved.
doi:10.1016/j.msea.2005.12.051

supplied by Rohn-Haas, Germany) for 24 h. The powders were then dried, crushed and sieved again. Pellets of 15 mm in diameter were isostatically pressed at 80 MPa. Finally, the pellets were sintered at 1300 °C for 3 h. In order to minimize the loss of lead due to vaporization, the PbO atmosphere during the sintering process was maintained using PZ as the spacer powder. The microstructures of the sintered samples were examined using a scanning electron microscopy (JEOL, JSM5910). The phase formation of the calcined powders and the sintered pellets were determined using a diffractometer (Philips ADP1700). The density of the sintered samples was measured by Archimedes' method with distilled water as the fluid medium. Effect of Ba^{2+} content on the mechanical properties of the ceramics was studied by Vickers and Knoop microhardness testers. Indentations were applied on the polished surfaces of PZ ceramics. Applied loads were 500 and 50 g for Vickers and Knoop microhardness, respectively, with an indentation period of 15 s. The sintered samples were prepared for electrical properties measurements by first polishing and then gold sputtering on to the clean pellet faces. The poling was done conventionally, in silicone oil bath at 170 °C with a field of 25 kV/cm. After poling, the d_{33} coefficient was measured using a d_{33} tester (Pennebaker Model 8000). The dielectric measurements were carried out at room temperature using an impedance analyzer (HIOKI 3532-50).

3. Results and discussion

X-ray diffraction (XRD) patterns of the calcined $(Pb_{1-x}Ba_x)ZrO_3$ powders for $0.00 \le x \le 0.30$ are shown in Fig. 1. Pure perovskite phase was observed for the whole range of the compositions. Also the XRD patterns indicate that the replacement of Pb^{2+} by Ba^{2+} ions apparently influenced the orthorhombic $PbZrO_3$ structure. For all of the samples, the diffraction lines could be indexed with respect to an orthorhombic structure. The intensity ratio of 0 0 4/2 4 0 peaks and the relative intensity of superlattice reflections, namely 1 1 0 and 1 3 0/1 1 2 are decreased with increasing of Ba^{2+} content as shown in Fig. 2. Pokharel et al. reported that the XRD pattern of orthorhombic antiferroelectric (A_O) phase presents the doublet of 2 4 0 and 0 0 4 reflections change to the single peak of 2 0 0 reflections for rhombohedral ferroelectric (F_R) phase [14–17]. For a purely orthorhombic pattern, $I_{004/240} \sim 0.5$ and this value decreases with increasing amounts of coexisting rhombohedral phase. In addition, the superlattice reflections, such as 1 1 0 and 1 3 0/1 1 2 of A_O phase, are absolutely disappeared for the F_R phase. Therefore, the structure of as-calcined powder also revealed that, the fraction of the orthorhombic phase decreases with increasing Ba^{2+} content.

Fig. 3 shows the typical sintered densities for various PBZ compositions. The bulk densities for all samples are higher than 97% of theoretical density. The bulk density continuously decreases with increasing Ba^{2+} content. The result was agreed with the work by Pokharel et al. [17]. In general, the bulk density of $PbZrO_3$–$BaZrO_3$ system decreases with increasing mole percent of $BaZrO_3$ (BZ). The theoretical density of the constituent compounds PZ and BZ are 8.055 and 6.229 g/cm^3, respectively [23,24], which can be used to calculate an empirical estimate of

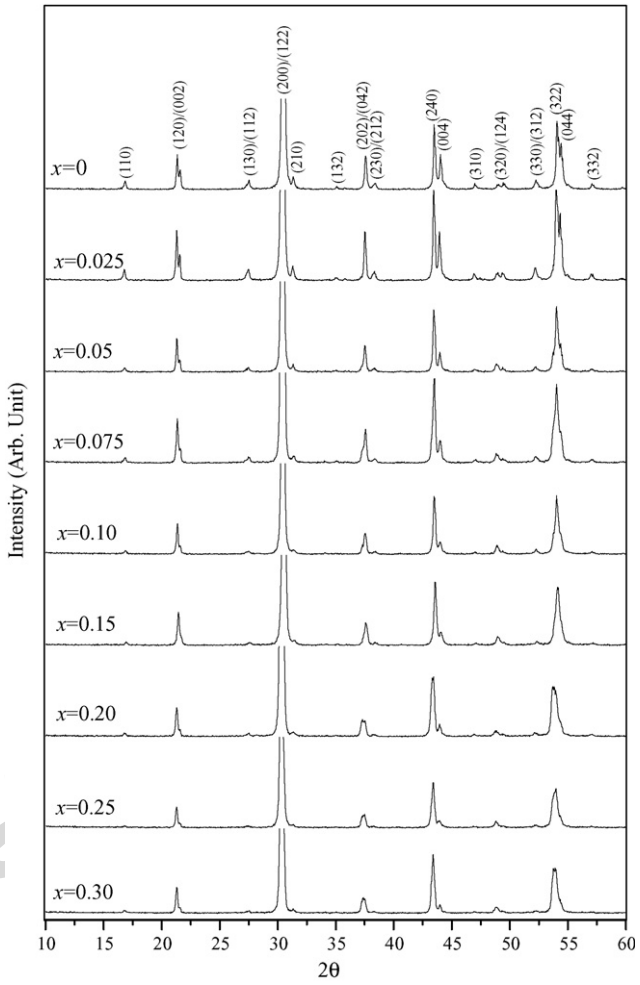

Fig. 1. XRD patterns of $(Pb_{1-x}Ba_x)ZrO_3$ calcined powders.

the density (D) via $D = 8.055(A - x) + 6.229x$. The variation of the measured density and the calculated density with composition x is also shown in Fig. 3.

The scanning electron micrographs in Fig. 4 show as-sintered surface of $(Pb_{0.975}Ba_{0.025})ZrO_3$ and $(Pb_{0.850}Ba_{0.150})ZrO_3$

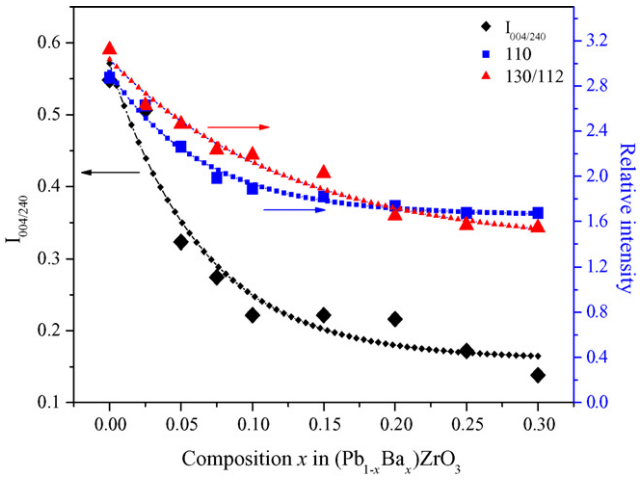

Fig. 2. Relative intensity of (1 1 0), (1 3 0)/(1 1 2) XRD peaks and value of intensity ratio, $I_{004/240}$ for calcined powders as a function of Ba^{2+} content.

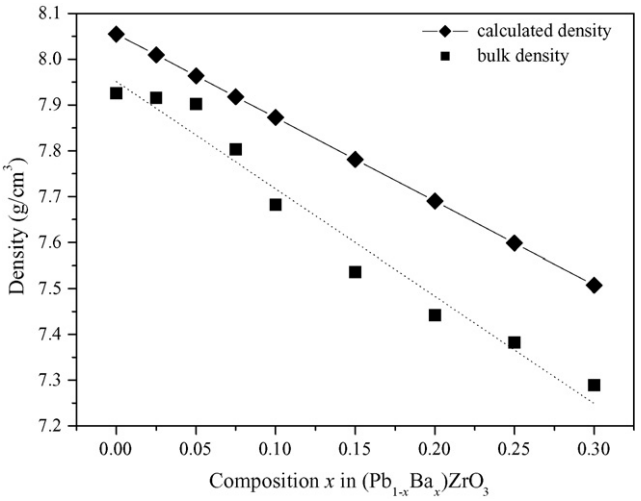

Fig. 3. Calculated density and bulk density of sintered pellets as a function of composition x.

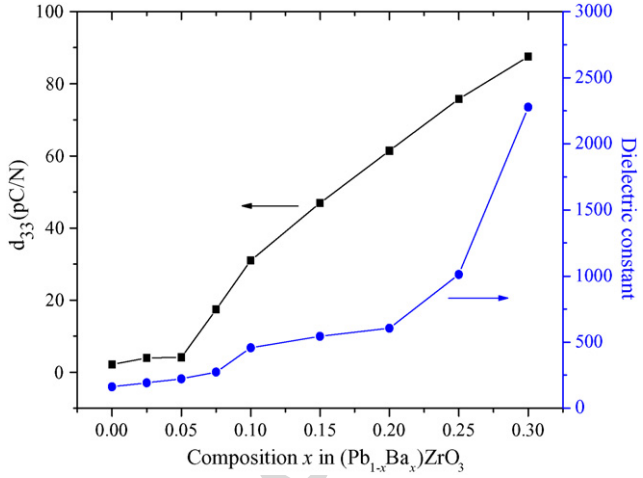

Fig. 5. Piezoelectric coefficient d_{33} and dielectric constant at room temperature of $(Pb_{1-x}Ba_x)ZrO_3$ ceramics with various x.

ceramics. It can be seen that the samples with higher Ba^{2+} concentration show more uniformity in grain size. The ceramics with $x = 0.00$–0.05 compositions show the grain size of 1.0–1.3 μm, while the $x = 0.075$–0.30 compositions show a grain size of 1.6–2.3 μm (as seen in Table 1). The effect of Ba^{2+} substitution on the mechanical properties of the samples was studied by using Vickers hardness, Knoop hardness, fracture toughness and Young's modulus. These values are listed in Table 1. It was found that there is no relation between Ba^{2+} concentration and the mechanical properties. Generally, the mechanical properties of lead base ceramics depend on many factors such as grain size and porosity [25]. The variation in mechanical properties is likely caused by the variation in grain size of the samples. Because of the samples were prepared by normal solid-state method, the variation in mechanical properties may also be attributed to chemical homogeneity effect.

The longitudinal piezoelectric sensitivity of $(Pb_{1-x}Ba_x)ZrO_3$ at room temperature are shown in Fig. 5. The d_{33} value gradu-

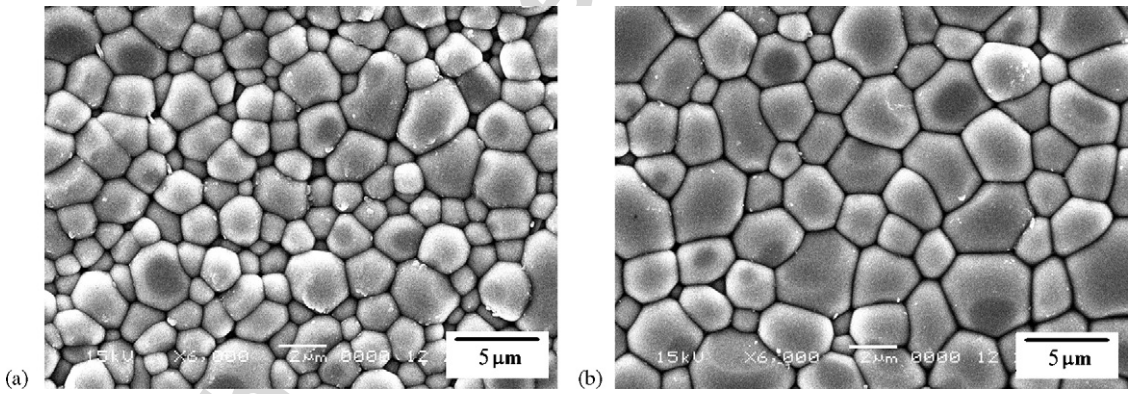

Fig. 4. Scanning electron micrographs of as-sintered surface of (a) $(Pb_{0.975}Ba_{0.025})ZrO_3$ and (b) $(Pb_{0.850}Ba_{0.150})ZrO_3$ ceramics.

Table 1
Average grain size and mechanical properties of $(Pb_{1-x}Ba_x)ZrO_3$ ceramics

Samples composition (nominal x)	Average grain size (μm)	Vickers hardness (GPa)	Knoop hardness (GPa)	Fracture toughness (MPa m$^{1/2}$)	Young's modulus (GPa)
0.000	1.0	4.81 ± 0.18	4.15 ± 0.48	3.29 ± 0.19	473 ± 55.06
0.025	1.3	6.48 ± 0.44	5.50 ± 0.77	2.09 ± 0.32	189 ± 39.76
0.050	1.3	5.83 ± 0.32	4.40 ± 0.37	1.83 ± 0.25	143 ± 41.63
0.075	2.3	5.61 ± 0.49	4.97 ± 0.35	2.32 ± 0.95	263 ± 151.10
0.100	1.6	5.85 ± 0.35	4.73 ± 0.33	1.58 ± 0.59	109 ± 116.26
0.150	2.0	5.10 ± 0.58	5.67 ± 0.31	2.75 ± 1.19	283 ± 152.60
0.200	1.7	4.61 ± 0.65	4.60 ± 0.26	2.33 ± 0.68	296 ± 87.24
0.250	1.7	5.30 ± 0.59	4.86 ± 0.53	2.65 ± 0.40	329 ± 94.04
0.300	2.2	4.10 ± 0.60	5.10 ± 0.37	2.15 ± 0.54	186 ± 74.95

ally increases with increasing Ba^{2+} content. Roberts [4] reported that the d_{33} value of $(Pb_{0.700}Ba_{0.300})ZrO_3$ was ~65 pC/N, and it is 10^{-1} pC/N for PZ [26]. The present result indicates that substitution Pb^{2+} by Ba^{2+} enhanced some piezoelectric property in PBZ.

The dielectric constant at 1 kHz as a function of Ba^{2+} concentration at room temperature is also shown in Fig. 5. The dielectric constant of the samples increases from ~160 to 2300 with increasing Ba^{2+} concentration from $x = 0.00$ to 0.30. This result suggests that the Ba^{2+} content in PBZ ceramics has a significant effect on the dielectric constant.

4. Conclusions

In the present work, effect of Ba^{2+} concentration on the properties of the PBZ ceramics was studied. The orthorhombic phase and the fraction of the antiferroelectric phase were found to decrease with increasing Ba^{2+} content. The results were corresponded to the structural phase changes in PBZ. The bulk density of PBZ ceramics continuously decreases with increasing Ba^{2+}content. This trend matches that of the calculated density of PZ-BZ system. The d_{33} value at room temperature gradually increases with increasing Ba^{2+} content. It is also indicated that substitution Pb^{2+} by Ba^{2+} enhanced some dielectric property of PBZ. However, there is no relation between Ba^{2+} concentration and the mechanical properties.

Acknowledgements

This work was supported by The Thailand Research Fund (TRF). The Authors would like to thank Prof. Dr. Tawee Tunkasiri for his help in many facilities.

References

[1] F.W. Ainger, Modern Oxide Materials, Academic Press, New York, USA, 1972, pp. 147–175.
[2] E. Sawaguchi, G. Shirane, S. Hoshino, Phys. Rev. 83 (1951) 1078.
[3] E. Sawaguchi, G. Shirane, Y. Takagi, J. Phys. Jpn. Soc. 6 (1951) 333–339.
[4] S. Roberts, J. Am. Ceram. Soc. 33 (1950) 63–66.
[5] L. Goulpeau, Sov. Phys. Solid St. 8 (1967) 1970–1971.
[6] V.J. Tennery, J. Am. Ceram. Soc. 49 (1966) 483–486.
[7] B.A. Scott, G. Burns, J. Am. Ceram. Soc. 55 (1972) 331–333.
[8] R.W. Whatmore, A.M. Glazer, J. Phys. C: Solid State Phys. 12 (1979) 1505–1516.
[9] G. Shirane, Phys. Rev. 86 (1952) 219–227.
[10] G. Shirane, S. Hoshino, Acta Cryst. 7 (1954) 203–210.
[11] I.H. Ismailzade, O.A. Samedov, Phys. Status Solidi (A) 90 (1985) 445–448.
[12] Z. Ujma, J. Handerak, M. Pawelczyk, D. Dmytrow, Ferroelectrics 129 (1992) 127–139.
[13] K.H. Yoon, S.C. Hwang, J. Mater. Sci. 32 (1997) 17–21.
[14] B.P. Pokharel, D. Pandey, J. Appl. Phys. 86 (1999) 3327–3332.
[15] B.P. Pokharel, D. Pandey, J. Appl. Phys. 88 (2000) 5364–5373.
[16] B.P. Pokharel, D. Pandey, J. Appl. Phys. 90 (2001) 2294–2985.
[17] B.P. Pokharel, M.K. Datta, D. Pandey, J. Mater. Sci. 34 (1999) 691–700.
[18] I. El-Harrad, P. Becker, C. Carabatos-Nedelec, J. Handerek, Z. Ujma, D. Dmytrow, Vib. Spectrosc. 10 (1996) 301–309.
[19] I. El-Harrad, A. Ridah, C. Carabatos-Nedelec, P. Becker, J. Handerek, Z. Ujma, D. Dmytrow, J. Raman Spectrosc. 29 (1998) 123–129.
[20] I. El-Harrad, A. Ridah, Ferroelectrics 265 (2002) 211–223.
[21] B.P. Pokharel, R. Ranjan, D. Pandey, Appl. Phys. Lett. 74 (1999) 756–758.
[22] B.P. Pokharel, D. Pandey, Phys. Rev. B 65 (2002) 214108.
[23] Powder Diffraction File No. 87-0570, International Centre for Diffraction Data, Newton Square, PA, 2000.
[24] Powder Diffraction File No. 06-0399, International Centre for Diffraction Data, Newton Square, PA, 2000.
[25] K. Uchino, Piezoelectric Actuators/Ultrasonic Motors, Kluwer Acadermic Publishers, Boston, USA, 1996, pp. 113–114.
[26] S. Roberts, Phys. Rev. 51 (1951) 1078.

Available online at www.sciencedirect.com
ScienceDirect
Current Applied Physics 7 (2007) 582–585
Current Applied Physics
An official journal of the KPS
www.elsevier.com/locate/cap
www.kps.or.kr

The improvement in dielectric and ferroelectric performance of PZT–PZN ceramics by thermal treatment

Naratip Vittayakorn [a,*], Gobwute Rujijanagul [b], David P. Cann [c]

[a] Department of Chemistry, Faculty of Science, King Mongkut's Institute of Technology Ladkrabang, Bangkok 10520, Thailand
[b] Department of Physics, Faculty of Science, Chiang Mai University, Chiang Mai 50200, Thailand
[c] Faculty of Materials Science, Department of Mechanical Engineering, Oregon State University, Corvallis, OR 97331, United States

Received 24 November 2006; accepted 5 December 2006
Available online 23 December 2006

Abstract

Pyrochlore-free lead zirconate titanate – lead zinc niobate ceramics have been systematically investigated in the as-sintered condition as well as after annealing. The ceramics were characterized by dielectric spectroscopy and Sawyer–Tower polarization (*P–E*) measurements. The powders of $Pb[(Zr_{1/2}Ti_{1/2})_{(1-x)}$–$(Zn_{1/3}Nb_{2/3})_x]O_3$, where $x = 0.1$, 0.3 and 0.5 were prepared using the columbite–(wolframite) precursor method. The general trend seems to indicate that the annealed samples become more normal-ferroelectric-like behavior as opposed to the relaxor-ferroelectric-like behavior observed in the as-sintered state. The as-sintered 0.9PZT–0.1PZN ceramic exhibited weak relaxor-ferroelectric behavior, with a relatively low dielectric constant maximum of 14,000 measured at 1 kHz. Annealing resulted in a transition to normal-ferroelectric-like behavior, a shift in the dielectric maximum temperature from 360 °C to 350 °C, and a dramatic increase in the dielectric constant at 1 kHz to a maximum value of 35,000 for the longer anneal. After thermal annealing at 900 °C for one week a strong enhancement of remanent polarization (P_r) was observed.

PACS: 77.84.Dy; 77.65.–j; 77.80.Bh

Keywords: Lead zinc niobate (PZN); Lead zirconate titanate (PZT); Dielectric properties

1. Introduction

Lead zirconate titanate (PZT) is one of the most interesting perovskite ferroelectric materials for applications in various devices owing to its potential usefulness and stability [1]. PZT have been applied to many useful electronic devices by utilizing their excellent dielectric, piezoelectric and pyroelectric properties [2]. Lead zirconate titanate ceramics and their solid solution with several complex perovskite oxides represented by $Pb(B'B'')O_3$ have been investigated [3–5]. Among the various complex ferroelectric oxide materials, several niobates with a transition point higher than room temperature are $Pb(Fe_{1/2}Nb_{1/2})O_3$ [6], $Pb(Mn_{1/2}Nb_{1/2})O_3$ [7], $Pb(Sc_{1/2}Nb_{1/2})O_3$ [8], $Pb(Zn_{1/3}Nb_{2/3})O_3$ [4], and $Pb(Cd_{1/3}Nb_{2/3})O_3$ [9]. Among them Lead zinc niobate [$Pb(Zn_{1/3}Nb_{2/3})O_3$, (PZN)] is also a typical ferroelectric relaxor material with a transition temperature of 140 °C and its ferroelectricity was reported by Smolenskii et al. in 1959 [10]. PZN is one of the most famous relaxor-ferroelectrics with perovskite structure exhibiting a diffused phase transition [11,12]. Single crystals of PZN can be synthesized by using flux method with excellent dielectric, optical, and electrostrictive properties, but PZN ceramics with pure perovskite are relatively difficult to prepare by conventional ceramic techniques [13,14]. Since both PZT and PZN have perovskite structure and are known to have excellent dielectric and piezoelectric properties, it is suggested that PZN alloyed with PZT to stabilize and optimize the PZN ceramics. Recently our previous work [4,15] has shown promise in producing

* Corresponding author. Tel.: +66 9 700 2136; fax: +66 2 3264415.
E-mail address: naratipcmu@yahoo.com (N. Vittayakorn).

1567-1739/$ - see front matter © 2007 Elsevier B.V. All rights reserved.
doi:10.1016/j.cap.2006.12.002

phase-pure perovskite PZN–PZT ceramics with the columbite method. A morphotropic phase boundary (MPB) between the PZN-rich rhombohedral phase and the PZT-rich tetragonal phase was reported at PZN:PZT 50/50 ~ 0.2:0.8. At this composition, a high dielectric constant (ε_r) ~ 26,000 was measured [16]. In this study we emphasize the effect of annealing on the crystal structure dielectric and ferroelectric properties in PZT–PZN ceramics. The samples were heat treated at 900 °C for one week in a sealed Al_2O_3 crucible with PbO-rich atmosphere. The temperature and frequency dependence of the dielectric constant are given for as-sintered and annealed samples. Finally, the remanent polarization and coercive field determined from *P–E* hysteresis loops are also introduced.

2. Experimental procedure

PZT-based ceramics with the composition of $Pb[(Zr_{1/2}Ti_{1/2})_{(1-x)}$–$(Zn_{1/3}Nb_{2/3})_x]O_3$, where $x = 0.1$, 0.3 and 0.5 were prepared by columbite–(woulframite) precursor. The reagent-grade oxide powders of PbO (99.9%, Aldrich, Milwaukee, WI, USA), ZnO (99.9%), Nb_2O_5 (99.9%), ZrO_2 (99.9%) and TiO_2 (99.9%) were used as starting raw materials. Prior to reaction with other raw materials, ZnO was reacted with Nb_2O_5 at 975 °C for 4 h to form $ZnNb_2O_6$ and ZrO_2 was reacted with TiO_2 at 1400 °C for 4 h to form $ZrTiO_4$. The precursors $ZnNb_2O_6$, $ZrTiO_4$ and PbO (with 2 mol% excess PbO) were weighted and mixed well by ball-milling in polyethylene bottle together with methyl alcohol and partially stabilized zirconia balls. Methyl alcohol was removed by heating at 80 °C for appropriate durations and then the mixture was dried at 150 °C for 24 h. After drying, the mixture powders were calcined at 700–900 °C for 4 h in covered Al_2O_3 crucible. To investigate densification of ceramics, the disks were sintered in a sealed alumina crucible at temperatures ranging from 1175 °C to 1275 °C using a heating rate of 5 °C/min and a dwell time of 2 h. To prevent PbO volatilization from the disks, a PbO atmosphere was maintained by placing $PbZrO_3$ powders in the crucible. This resulted in pellets with 94–96% of theoretical density which were single-phase perovskite with grain sizes of 2–5 μm. The crystal structure and phase transition of the individual compositions can be found in Refs. [4,17]. To determine the effect of thermal annealing, the maximum density sample was thermally annealed at 900 °C in the same PbO atmosphere for one week.

The dielectric and ferroelectric properties of the as-sintered and annealed samples were characterized as follows. The polished samples were electroded with silver paste and then fired at 550 °C for 30 min. The dielectric constant (K) and dielectric loss (tan δ) were measured on heating at 3 °C min^{-1} using an LCR meter (HP4284A, Hewlett-Packard, Palo Alto, CA) over the range of 100–500 kHz and temperatures 25–450 °C. In addition, the polarization (P) was measured as a function of electric field (E), using a ferroelectric tester system (Radiant Technologies, Inc., PT66A).

3. Results and discussion

The phase development in the annealed samples was analyzed by XRD and the results are shown in Fig. 1. All samples show single-phase powder diffraction pattern. No secondary reaction phases, such as PbO, Pb-based compounds, unreacted oxide and so on, are observed in the pattern. There seem to be no measurable changes before and after annealing. Fig. 2a–c show the dielectric constant versus temperature of the as-sintered and annealed samples of compositions $x = 0.1$, 0.3 and 0.5, respectively, for frequency of 100 Hz, 1 kHz, 10 kHz, 100 kHz and 500 kHz. The as-sintered sample showed typical relaxor-ferroelectric-like behavior, characterized by a diffuse dielectric-temperature response (Fig. 2a). After annealing, a significant improvement in the dielectric constant is observed, especially near the temperature of the maximum dielectric constant and it is relatively small at room temperature and at temperatures far above T_m. At the composition $x = 0.1$, the maximum dielectric constant at 1 kHz (K_m @ 1 kHz) was approximately 14,000 and the T_m value was 360 °C. The general trend seems to indicate that the annealed samples become more normal-ferroelectric-like behavior as opposed to the relaxor-ferroelectric-like behavior observed in the as-sintered state. In contrast, the annealed samples showed normal-ferroelectric behavior, characterized by a much-sharper dielectric-temperature response and a weak dependence of T_m with frequency. Annealing resulted in a transition to normal – ferroelectric – like behavior, a shift in the dielectric maximum temperature from 360 °C to 350 °C, and a dramatic increase in the dielectric constant at 1 kHz to a maximum value of 35,000, up from the initial value of 14,000 for as-sintered sample. This behavior also appeared in the

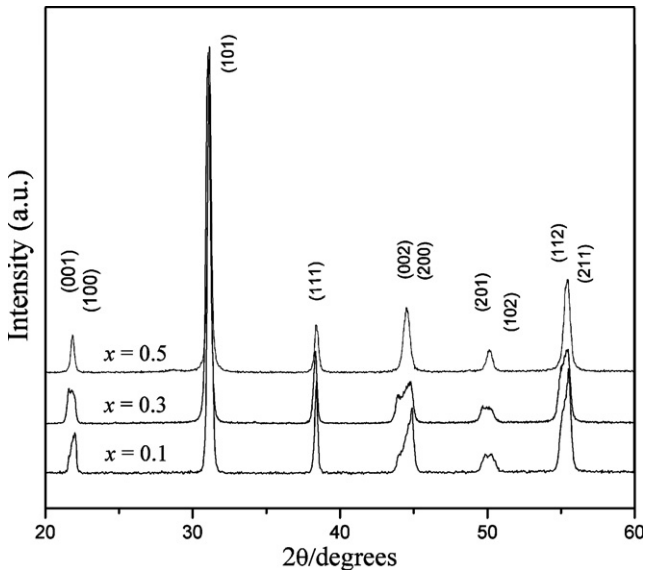

Fig. 1. X-ray diffractograms of annealed samples for various compositions of the $Pb[(Zr_{1/2}Ti_{1/2})_{(1-x)}$–$(Zn_{1/3}Nb_{2/3})_x]O_3$, where $x = 0.1$, 0.3 and 0.5 system at room temperature.

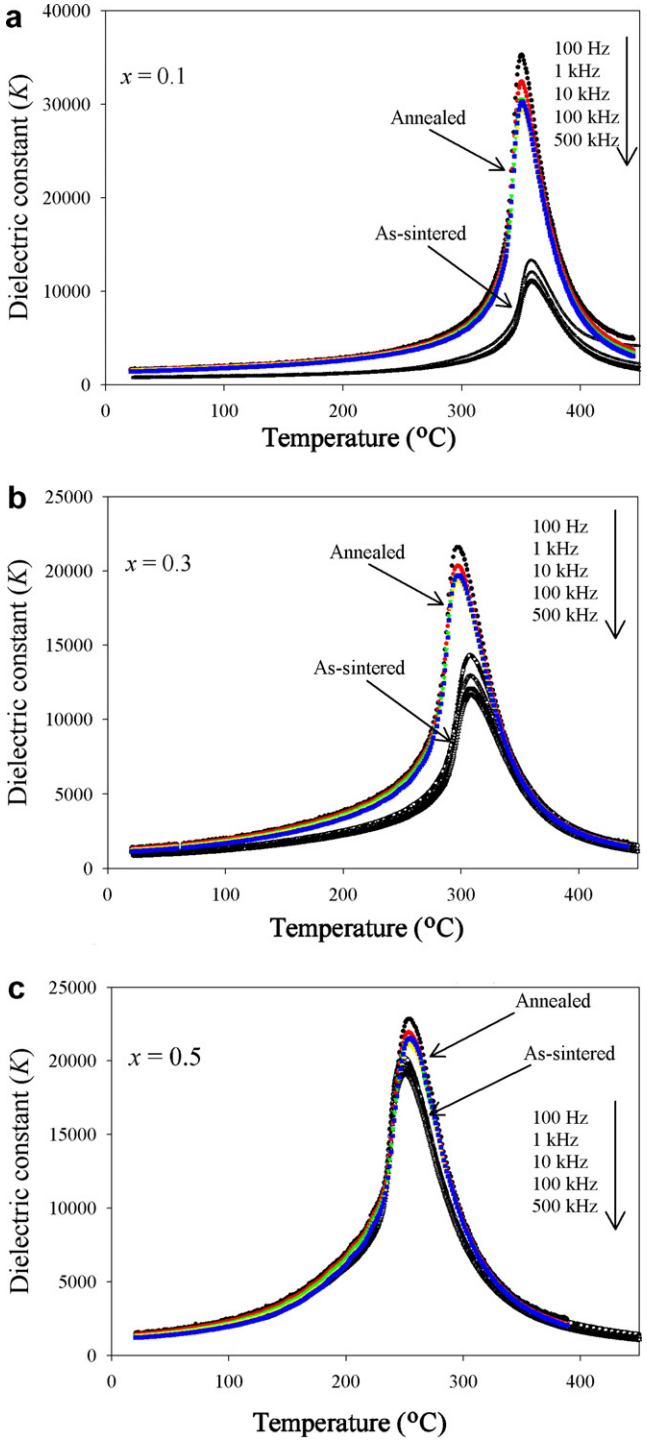

Fig. 2. Temperature dependence of the dielectric constant at difference frequencies for as-sintered and annealed samples (a) $x = 0.1$, (b) $x = 0.3$ and (c) $x = 0.5$.

$x = 0.3$ and 0.5 composition. The dielectric constant and transition temperature of the samples studied is summarized in Table 1. However, very limited improvements were observed for the $x = 0.5$ composition because the higher PZN content required lower sintering temperatures, thus limiting the efficacy of the annealing step. Polarization hysteresis measurements at room temperature were performed

Table 1
Dielectric properties of as-sintered and annealed sample

Composition	As-sintered		Annealed	
	K_m	T_m,°C	K_m	T_m,°C
$x = 0.1$	14,000	360	35,000	350
$x = 0.3$	14,500	310	21,500	300
$x = 0.5$	21,000	250	23,000	254

using a modified Sawyer–Tower circuit. Fig. 3 shows the saturated loops of 0.7PZT–0.3PZN samples with difference electric fields strengths.

It is clearly evident that the shape of hysteresis various greatly with the electric fields strength. At 5 kV/cm electric fields strength, a near-linear relationship of P–E is observed. This result is due to the fact that the electric field is not large enough to switch any domains. At 10 kV/cm electric fields, the polarization nonlinearity is developed in both regions of the positive and negative fields. These results clearly demonstrate that the electric field strength of 10 kV/cm is of enough energy to constrain realignment of some domains in the direction of the applied fields. No evidence of pinning effect or asymmetric loop was detected in all electric fields strength. At 30 kV/cm electric field strength, the loop reveals fully developed symmetric hysteresis loop. This shows that the electric fields strength of 30 kV/cm has of enough energy to constrain realignment of all domains in the direction of the electric fields. The hysteresis loops of as-sintered and annealed samples are shown in Fig. 4. The as-sintered sample exhibited a smaller remnant polarization (P_r) and lower coercive field (E_c), compared with the annealed samples. Annealed sample showed normal-ferroelectric behavior with a rectangular loop. For the composition $x = 0.3$, the P_r increased from 21.4 μC/cm^2 to 34.7 μC/cm^2 for the annealed sample. Moreover the E_c decreased from 14.5 kV/cm to 12.3 kV/cm after annealing. Although this behavior was observed in all of our composition, the increasing in the P_r and

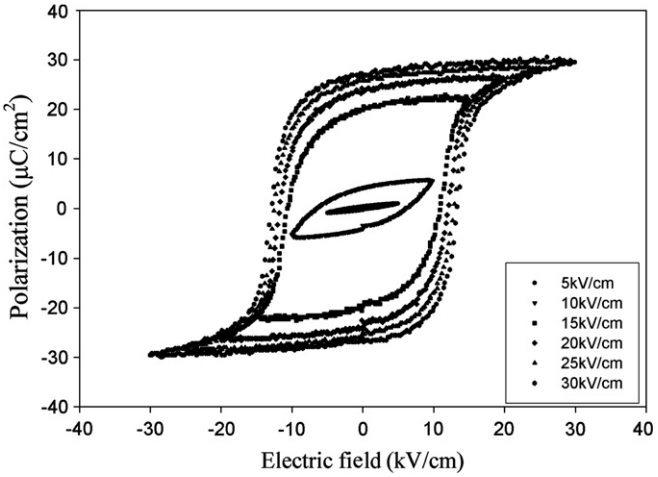

Fig. 3. P–E behaviors for annealed sample at various maximum electric field strengths.

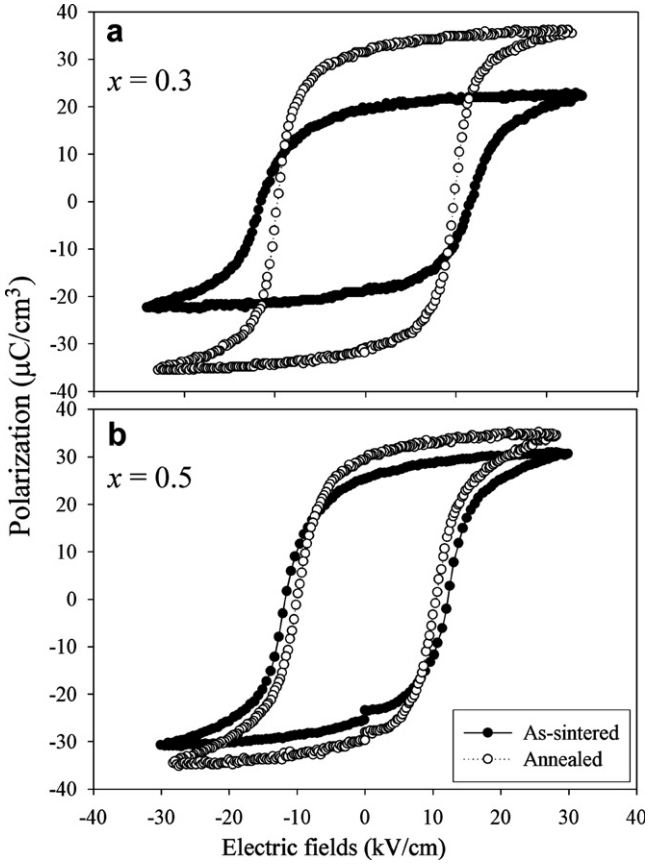

Fig. 4. *P–E* behaviors for $(1-x)$PZT–xPZN ceramics before and after annealing.

decreasing in the E_c was minimal at high concentrations of PZN. This is due to the fact that the higher PZN content required lower sintering temperatures to achieve the best combination of density and properties. Therefore, heat treatment is not necessary for ceramics with high PZN content. This change in behavior is might be due to the extrinsic effect of domain wall motion and a decrease in the chemical heterogeneity of the samples. This behavior is consistent with the conclusions of Xia et al. [18] and Leite et al. [5] in the PZN–BT–PT and PMN–PT system respectively.

4. Conclusions

The dielectric and ferroelectric properties of $Pb[(Zr_{1/2}Ti_{1/2})_{(1-x)}$–$(Zn_{1/3}Nb_{2/3})_x]O_3$, where $x = 0.1$, 0.3 and 0.5 ceramics formed via the columbite process were investigated. Thermal treatment is an effective way to improve the dielectric and piezoelectric responses of PZT–based ferroelectric ceramics. The annealing time has an effect on the electrical properties. The large improvement in the dielectric and ferroelectric properties due to annealing are mainly attributed to the increase in the chemical homogeneity and the extrinsic effect of domain wall motion in ferroelectric ceramics.

Acknowledgements

The authors are grateful to the Thailand Research Fund (TRF), the Commission on Higher Education (CHE), Faculty of Science Chiang Mai University, and King Mongkut's Institute of Technology Ladkrabang for their financial support.

References

[1] K. Uchino, Ferroelectric Devices, Marcel Dekker, New York, 2000.
[2] Y. Xu, Ferroelectric Materials and Their Application, Elsevier Science Publishers B.V., 1991.
[3] N. Vittayakorn et al., The morphotropic phase boundary and dielectric properties of the xPb$(Zr_{1/2}Ti_{1/2})O_3$–$(1-x)$Pb$(Ni_{1/3}Nb_{2/3})O_3$ perovskite solid solution, J. Appl. Phys. 96 (9) (2004) 5103.
[4] N. Vittayakorn et al., Influence of processing condition on the phase transition and ferroelectric properties of Pb$(Zn_{1/3}Nb_{2/3})O_3$–b$(Zr_{1/2}Ti_{1/2})O_3$ ceramics, Mat. Sci. Eng. B. 108 (2004) 258.
[5] E.R. Leite et al., Chemical heterogeneity in PMN–35PT ceramics and effects on dielectric and piezoelectric properties, J. Am. Ceram. Soc. 85 (12) (2002) 3018.
[6] Y. Yoshikawa, Crystallization behavior of PZN–PFN powders from nitrate solutions, J. Eur. Ceram. Soc. 19 (6–7) (1999) 1037–1041.
[7] Y. Yamashita, N. Ichinose, Can relaxor piezoelectric materials outperform PZT? (Review), Proc. IEEE ISAF'96. (1996) 71.
[8] V.A. Isupov, Causes of phase-transition broadening and the nature of dielectric polarization relaxation in some ferroelectric, Sov. Phys. Solid state. 5 (1) (1958) 136.
[9] N. Ichinose, T. Takahashi, Y. Tokomizo, J. Phys. Soc. Jpn. 31 (1971) 1848.
[10] G.A. Smolenskii, A.L. Agranovskaya, Dielectric polarization of and lossed of some complex compounds, Sov. Phys.-Tech. Phys (1958) 1380.
[11] M.L. Mulvihill et al., Domain-related Phase transition like behavior in lead zinc niobate relaxor ferroelectric single crystals, J. Am. Ceram. Soc. 80 (16) (1997) 1462.
[12] L.E. Cross, Relaxor ferroelectrics: An Overview, Ferroelectrics 151 (1994) 305.
[13] A. Halliyal et al., Dielectric and ferroelectric properties ceramics in the PZN–BT–PT system, J. Am. Ceram. Soc. 70 (2) (1987) 119–124.
[14] T.R. Shrout, A. Halliyal, Proparation of lead-based ferroelectric relaxors for capacitors, Am. Ceram. Soc. Bull. 66 (4) (1987) 704.
[15] N. Vittayakorn et al., Piezoelectric properties of $(1-x)$Pb$(Zr_{1/2}Ti_{1/2})O_3$–xPb$(Zn_{1/3}Nb_{2/3})O_3$ ceramics prepared by the columbite–(wolframite) precursor method, Curr. Appl. Phys. 6 (3) (2006) 303–306.
[16] N. Vittayakorn et al., Dielectric properties and morphotropic phase boundary in the xPb$(Zn_{1/3}Nb_{2/3})O_3$–$(1-x)$Pb$(Zr_{0.5}Ti_{0.5})O_3$ pseudo-binary system, J. Electroceramic. 16 (2) (2006) 141–149.
[17] N. Vittayakorn et al., Dielectric and ferroelectric characteristics of 0.7 PZT–0.3PZN ceramics substituted with Sr., J. Phys. D: Appl. Phys. 38 (2005) 2942–2946.
[18] F. Xia, X. Yao, Postsintering annealing induced extrinsic dielectric and piezoelectric responses in lead-zinc-niobate-based ferroelectric ceramics, J. Appl. Phys. 92 (5) (2002) 2709–2715.

Phase Transitions,
Vol. 80, No. 3, March 2007, 209–215

Taylor & Francis
Taylor & Francis Group

Phase transition and linear thermal expansion of $(Pb_{1-x}Ba_x)ZrO_3$ ceramics

G. RUJIJANAGUL† and T. BONGKARN*‡

†Faculty of Science, Department of Physics, Chiang Mai University, Chiang Mai 50200, Thailand
‡Faculty of Science, Department of Physics, Naresuan University, Pitsanuloke 65000, Thailand

(*Received 17 October 2006; in final form 2 November 2006*)

$(Pb_{1-x}Ba_x)ZrO_3$ ceramics for the composition range $0 \leq x \leq 0.30$ were prepared by the mixed oxide solid state reaction method. Phase transition was studied by dielectric and dilatometric measurements. The ferroelectric to paraelectric phase transition temperature was progressively shifted to a lower temperature by replacing lead with barium. The $x = 0.20$ sample showed the maximum dielectric constant of 16,300 at the transition temperature. For compositions $0 \leq x \leq 0.075$, the antiferroelectric to ferroelectric phase transition exhibited a large linear thermal expansion. However, the antiferroelectric to ferroelectric phase transition did not exist for $0.10 \leq x \leq 0.30$ samples. A phase diagram for PBZ ceramics prepared by the conventional mixed oxide method was also present.

Keywords: $(Pb_{1-x}Ba_x)ZrO_3$; Phase transition; Dielectric properties; Linear thermal expansion

1. Introduction

$PbZrO_3$ (PZ) is a perovskite crystal, which was identified as antiferroelectric material. PZ exhibits three phases: an orthorhombic antiferroelectric (AFE) phase between room temperature and 230°C, a rhombohedral ferroelectric (FE) phase up to 233°C and a cubic paraelectric (PE) phase above 233°C [1–5]. The ferroelectric phase between 230–233°C is sometimes called the ferroelectric intermediate phase. The phase transitions between AFE to FE (AFE → FE) and FE to PE (FE → PE) in PZ have been extensively studied by previous authors [4, 5]. It is also reported that many properties of PZ are changed by incorporation of Ba^{2+} ions into the Pb^{2+} site of PZ [6–12]. The modification of PZ becomes $(Pb_{1-x}Ba_x)ZrO_3$ (PBZ) and exhibits the better dielectric properties compared with the pure PZ. By varying Ba^{2+} concentrations, electric fields, and temperatures in PBZ, many phase diagrams have been proposed [8, 9, 12]. It should be noted that different research groups reported different results and different phase diagrams. Further, the information for thermal

*Corresponding author. Email: researchcmu@yahoo.com

Phase Transitions
ISSN 0141-1594 print/ISSN 1029-0338 online © 2007 Taylor & Francis
http://www.tandf.co.uk/journals
DOI: 10.1080/01411590601098818

expansion associated with the phase transitions of PBZ ceramics is unclear. In the present work, $(Pb_{1-x}Ba_x)ZrO_3$ ceramics for $0 \leq x \leq 0.30$ were prepared by the mixed oxide solid state reaction method. X-ray diffraction, dielectric and dilatometric techniques were used to study the details of the phase transitions. Eventually, the phase diagram of PBZ system was constructed and compared to the previous work.

2. Experimental procedure

PBZ ceramics can be prepared by many methods [8, 9, 12]. However, in the present work, PBZ ceramics were prepared by a mixed oxide solid state reaction method as described by previous study [13]. The raw materials of PbO, ZrO_2 and $BaCO_3$ were weighed according to the formula $(Pb_{1-x}Ba_x)ZrO_3$, where $0 \leq x \leq 0.30$. The powders were mixed with acetone for 24 h using zirconia balls as the grinding media. The mixed powders were calcined at 1000°C for 1 h. The calcined powders were reground by wet ball-milling with 1 wt% binder for 24 h. The calcined powders with binder were isostatically pressed at 80 MPa into a pellet of 15 mm in diameter. Finally, the pellets were fired in an alumina crucible and sintered at 1300°C for 3 h. It is known that excess PbO affect the properties of lead base ceramics [14]. There is a loss of lead due to vaporization. Therefore, the PbO atmosphere for the sintering was maintained using $PbZrO_3$ as the spacer powder. Phase formation of the samples was determined by X-ray diffraction (XRD). For electrical measurement, the sintered samples were polished and then gold was sputtered on to the clean pellet faces. The dielectric measurement was carried out at 1 kHz using an impedance analyzer. The linear thermal expansion was measured using a dilatometer.

3. Results and discussion

Figure 1 shows XRD patterns of $(Pb_{1-x}Ba_x)ZrO_3$ calcined powders. The XRD traces showed diffraction profiles as attributed to pure PBZ [11]. Due to peak overlap effects between rhombohedral and orthorhombic structures, the intensity of the peak indexed as 240 in the orthorhombic pattern increased relative to the neighboring 004 peak with the presence of the rhombohedral phase [10]. This result indicates that the introduction of Ba^{2+} increases the proportion of the rhombohedral phase in PBZ calcined powders.

XRD patterns of ceramic samples are shown in figure 2. The XRD patterns for the composition of $0 \leq x \leq 0.10$ are qualitatively similar to that observed for the as-calcined powder. Although a similar situation prevails for the calcined powder, the sintered sample is predominantly rhombohedral whereas the calcined powder has a significant proportion of the orthorhombic phase as evidenced by the relative intensity of the 240 and 004 reflections. Due to the 004 reflection of orthorhombic phase completely vanished, but some of the superlattice reflections such as 110 and 230/212 were still present. For composition $x = 0.15$, the XRD results could be indicated that both rhombohedral and orthorhombic phases coexisted. The rhombohedral 200 reflection, which was a doublet in the calcined powder, has become a single peak for composition $0.20 \leq x \leq 0.30$. Also the

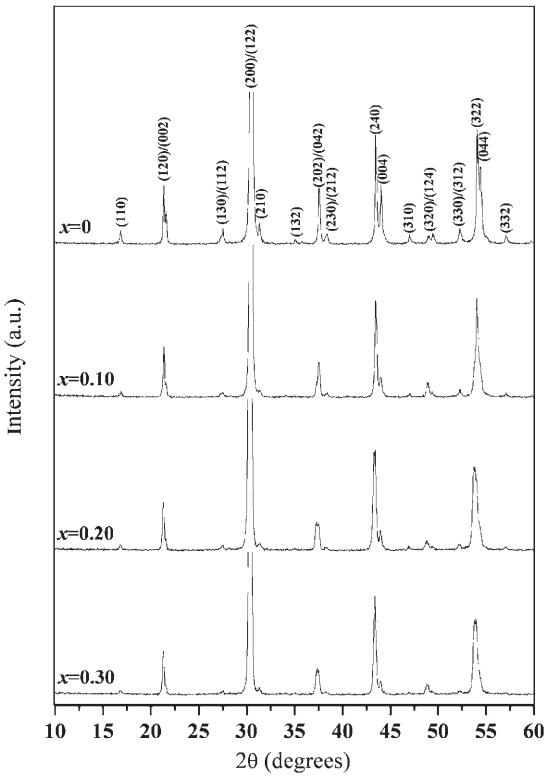

Figure 1. XRD patterns of calcined powders of $(Pb_{1-x}Ba_x)ZrO_3$.

superlattice lines of the orthorhombic phase have completely vanished in the pellets. This clearly indicates that the structure is rhombohedral for $0.20 \leq x \leq 0.30$ ceramic samples.

Figure 3 shows the variation of dielectric constant with temperature of samples for $0 \leq x \leq 0.30$. The anomalies around 193, 157, and 116°C for $x = 0.025$, 0.050 and 0.075, respectively, are found. These anomalies are due to a transition from the AFE phase to FE phase [9]. However, no dielectric anomaly corresponding to the AFE $\rightarrow$ FE transition is observed, for $x \geq 0.10$. The AFE $\rightarrow$ FE transition temperature decreases at about the rate of 15.4°C/mol% of $BaZrO_3$ with respect to its value for pure PZ. The dielectric maximum of lead zirconate is shown to be shifted to a lower temperature by replacing lead with barium. The dielectric maximum in all samples, is linked with the transition of the FE phase to the PE phase [9, 12]. The FE $\rightarrow$ PE transition temperature was found to decrease from 232°C for the $x = 0$ sample to 82°C for the $x = 0.3$ sample with a rate of 4.8°C/mol% of $BaZrO_3$. The shift of transition temperature may be explained by the change of structure in PBZ with increasing Ba^{2+} [12].

The value of the maximum dielectric constant as a function of a Ba^{2+} concentration is shown in figure 4. The maximum dielectric constant increases with increasing Ba^{2+} content from 6300 for pure PZ to 16300 for PBZ20 ($x = 0.20$) for the FE $\rightarrow$ PE transition. At higher concentrations of Ba^{2+} substitution, the lowering of the maximum dielectric value is accompanied by a progressive

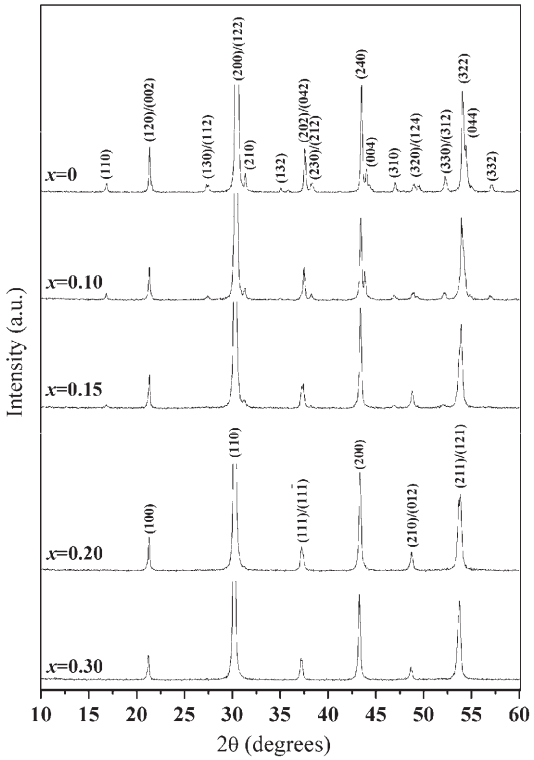

Figure 2. XRD patterns of as-sintered pellets of $(Pb_{1-x}Ba_x)ZrO_3$.

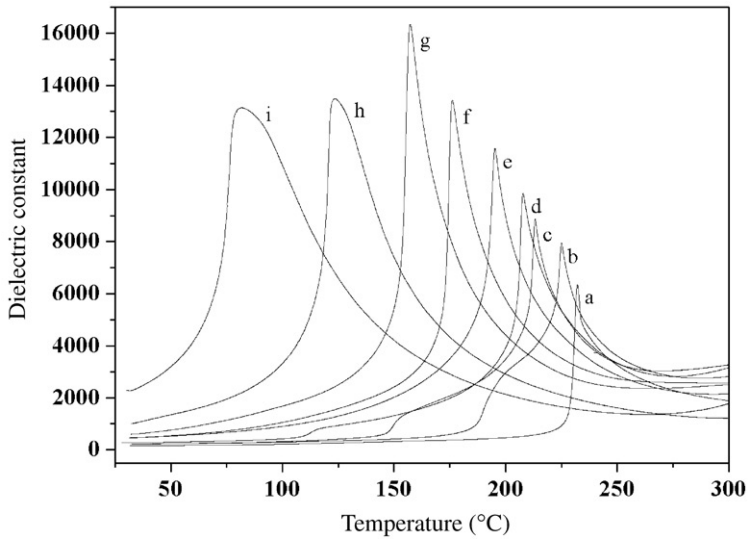

Figure 3. Dielectric constant *vs.* temperature of $(Pb_{1-x}Ba_x)ZrO_3$ ceramics; (a) $x=0$, (b) $x=0.025$, (c) $x=0.05$, (d) $x=0.075$, (e) $x=0.10$, (f) $x=0.15$, (g) $x=0.20$, (h) $x=0.25$, (i) $x=0.30$.

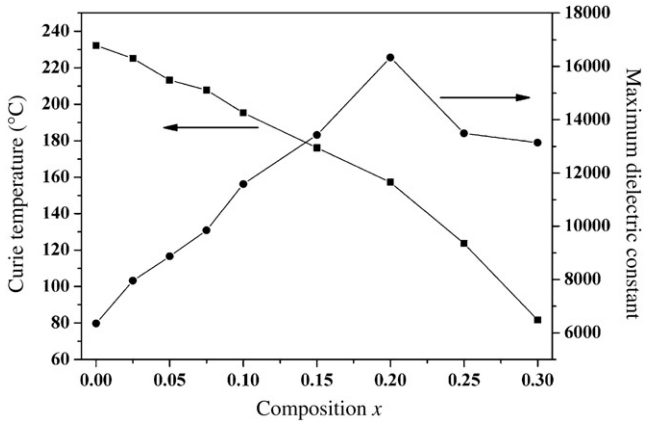

Figure 4. Curie temperature and maximum dielectric constant of $(Pb_{1-x}Ba_x)ZrO_3$ ceramics.

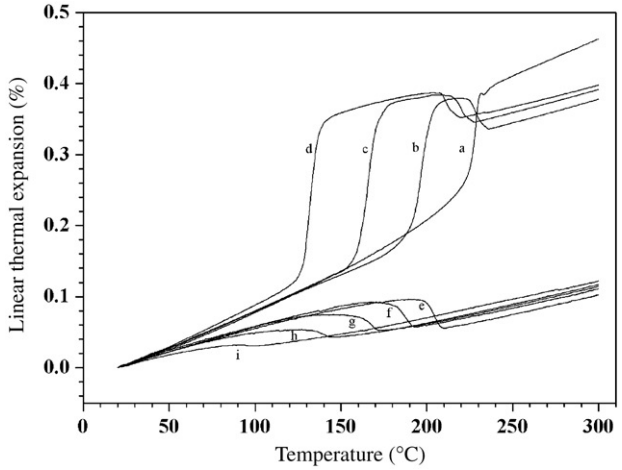

Figure 5. Linear expansion *vs.* temperature of $(Pb_{1-x}Ba_x)ZrO_3$ ceramics; (a) $x=0$, (b) $x=0.025$, (c) $x=0.05$, (d) $x=0.075$, (e) $x=0.10$, (f) $x=0.15$, (g) $x=0.20$, (h) $x=0.25$, (i) $x=0.30$.

broadening of the permittivity peak. The change in the dielectric constant can be related to the change of portion of coexist phase, i.e. the proportion of rhombohedral phase in PBZ increases with increasing Ba^{2+} content.

The measurement of the length of a specimen compared to its temperature is a method for the determination of the kinetics of the phase transformation of PBZ. The dilatometric thermal expansion of polycrystalline samples of $(Pb_{1-x}Ba_x)ZrO_3$, is plotted in figure 5. The presence of such a break in the thermal expansion curves indicates a phase transition. The discontinuous curves can be attributed to the AFE $\rightarrow$ FE and FE $\rightarrow$ PE phase transition with rising temperatures [4, 8]. By progressively increasing barium content, the AFE $\rightarrow$ FE and the FE $\rightarrow$ PE transition temperatures continuously decreased. For $x=0$, 0.025, 0.050 and 0.075, the linear thermal expansion curve transforms from the AFE phase to the FE phase through the transition region around 226, 189, 160 and 127°C, respectively. For $x=0.10$–0.30 samples, the AFE $\rightarrow$ FE transition does not exist. For FE $\rightarrow$ PE

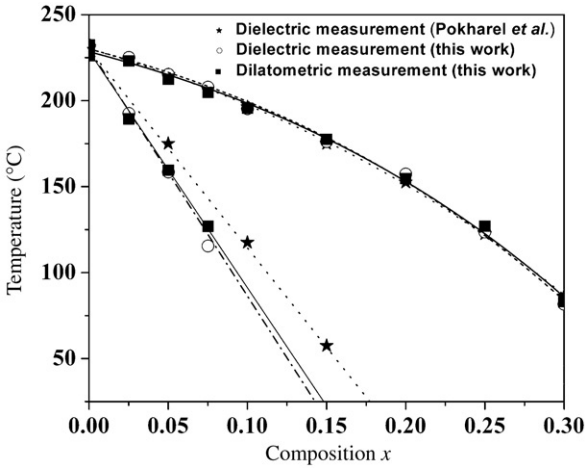

Figure 6. Phase diagram of $(Pb_{1-x}Ba_x)ZrO_3$ system made from the results of this work and Pokharel *et al*. work [12].

transition, the transition temperature decreases from 232°C for the $x = 0$ sample to 83°C for the $x = 0.30$ sample. It can be noted that the AFE → FE transition was accompanied by a large volume expansion while FE → PE transformation was accompanied by a small volume contraction.

A phase diagram of the PBZ system is shown in figure 6. It is clearly seen that the width of temperature range of the FE phase continuously increases with progressively increasing Ba^{2+} content. The FE → PE transition temperature in this work is consistent with the previous work [9, 12]. However, the AFE → FE transition temperatures are lower than those of the PBZ which was prepared by a chemical method [12]. This indicates that the processing method used to prepare the PBZ may be important in influencing the AFE → FE transition temperatures.

4. Conclusion

The phase transitions of PBZ ceramics prepared by a solid-state method, were studied by XRD, dielectric, and dilatometric measurements. A phase diagram of the PBZ system was present. The AFE → FE and FE → PE transition temperatures were found to decrease with increasing Ba^{2+} concentrations. However, the AFE → FE transition temperature was found to be lower than that of the PBZ prepared by chemical method. From the dilatometric measurement, the AFE → FE phase transition showed a large linear thermal expansion while the FE → PE phase transition was accompanied by a small contraction. In addition, the AFE → FE phase transition was not observed for compositions $0.10 \leq x \leq 0.30$.

Acknowledgements

The authors are grateful to the Thailand Research Fund, Graduate School Chiang Mai University, Faculty of Science, Chiang Mai University, Faculty of Science, Naresuan University and Commission on Higher Education (CHE), Thailand for

financial support. Thanks are also due to Prof. Dr Tawee Tunkasiri for his help with providing many facilities.

References

[1] S. Roberts, J. Am. Ceram. Soc. **33** 63 (1950).
[2] L. Goulpeau, Sov. Phys. Solid State **8** 1970 (1967).
[3] V.J. Tennery, J. Am. Ceram. Soc. **49** 483 (1966).
[4] B.A. Scott and G. Burns, J. Am. Ceram. Soc. **55** 331 (1972).
[5] R.W. Whatmore and A.M. Glazer, J. Phys. C: Solid State Phys. **12** 1505 (1979).
[6] G. Shirane and S. Hoshino, Acta Crystallogr. **7** 203 (1954).
[7] B.P. Pokharel, M.K. Datta and D. Pandey, J. Mater. Sci. **34** 691 (1999).
[8] G. Shirane, Phys. Rev. **86** 219 (1952).
[9] K.H. Yoon, S.C. Hwang and D.H. Kang, J. Mater. Sci. **32** 17 (1997).
[10] B.P. Pokharel and D. Pandey, J. Appl. Phys. **86** 3327 (1999).
[11] B.P. Pokharel and D. Pandey, J. Appl. Phys. **90** 2985 (2001).
[12] B.P. Pokharel and D. Pandey, J. Appl. Phys. **88** 5364 (2000).
[13] T. Bongkarn and G. Rujijanagul, Curr. Appl. Phys. **6** 319 (2006).
[14] T. Bongkarn, G. Rujijanagul and S.J. Milne, Mater. Lett. **59** 1200 (2005).
[15] W.Y. Pan, Q. Zhang and A. Bhalla, J. Am. Ceram. Soc. **72** 570 (1989).
[16] S.-E. Park, M.-J. Pan, K. Markowski, *et al*., J. Appl. Phys. **82** 1798 (1997).

Ferroelectrics, 345:109–114, 2006

ISSN: 0015-0193 print / 1563-5112 online
DOI: 10.1080/00150190601021337

Taylor & Francis
Taylor & Francis Group

Piezoceramic-Polymer Composites for Detector Applications**

PREUKSA AUISUI,[1] SUPASAROTE MUENSIT,[1,*] IAN L. GUY,[2] GOBWUTE RUJIJANAGUL,[3] AND TAWEE TUNKASIRI[3]

[1]Materials Physics Research Unit, Department of Physics, Prince of Songkla University, Hatyai 90112, Thailand
[2]Department of Physics, Macquarie University, NSW 2109, Australia
[3]Electroceramics Laboratory, Department of Physics, Chiangmai University, Chiangmai 50200, Thailand

Ferroelectric powders of $PbTiO_3$ were fabricated and sintered at low-temperatures. The ceramic pores were filled with an epoxy using a vacuum impregnation technique. SEM analysis showed a composite with 3–3 connectivity. The piezoelectric coefficient of the composite was evaluated as $(6.0 \pm 1.0) \times 10^{-12}$ m/V by an interferometric technique. The pyroelectric coefficient was 23 $\mu C/m^2{}^\circ C$. The pyroelectric detector properties and figures-of-merit of the composite are reported.

Keywords composite; piezoelectric; pyroelectric; interferometric; IR detector; thermal detector

Introduction

Piezoceramic-polymer composites with various connectivity patterns [1] are now an alternative to conventional piezoelectric materials. Owing to the advantages over other materials in terms of cost and ease of manufacture, epoxy-based composites were of interest in this work. Fine grained ceramic of Lead Titanate ($PbTiO_3$:PT) was fabricated to produce a porous PT the pores of which were impregnated with an epoxy. The PT-epoxy composites were tested as materials for pyroelectric long wavelength infrared (IR) radiation detectors [2]. The important parameters investigated were the strain piezoelectric coefficient, the pyroelectric coefficient, the thermal diffusivity, the voltage responsivity, the specific detectivity, and the three figures-of-merit.

Materials and Methods

Sample Preparation

In order to prepare PT powders, commercial powders of lead oxide (PbO) and titanium oxide (TiO_2) supplied by Fluka Ltd. were mixed and wet-ball milled for 24 h. The mixture

Received in final form September 5, 2006.
*Corresponding author. E-mail: supasarote.m@psu.ac.th
**Originally presented at AMF-4, Bangalore, India; December 12–15; 2003.

was dried before sieving, then calcined at 750°C for 2 h. The X-ray diffraction pattern analysed by a PHILIPS X'Pert MPD diffractometer confirmed the tetragonal phase of the calcined powders. The calcined powders were crushed and sieved into an alumina crucible for sintering at 1150°C to produce a porous-structure ceramic. The ceramic voids were filled with an epoxy by a vacuum impregnation technique at room temperature. The PT-epoxy composite was cut into disk samples and surface finished by grinding and polishing. The density of the sample was found to be 4.4×10^3 kg/m^3 so the volume fractions of ceramic: epoxy was determined to be 50:50.

The microstructure morphology of the composite was studied using a JEOL JSM-5200 scanning electron microscope (SEM). In order that the SEM micrographs would show the regions of the PT ceramic and epoxy more clearly, the micrographs were made on the polished surface before and after the epoxy was etched with acetone. As seen in Fig. 1, each phase was almost completely interconnected. Therefore, this composite had a 3–3 connectivity.

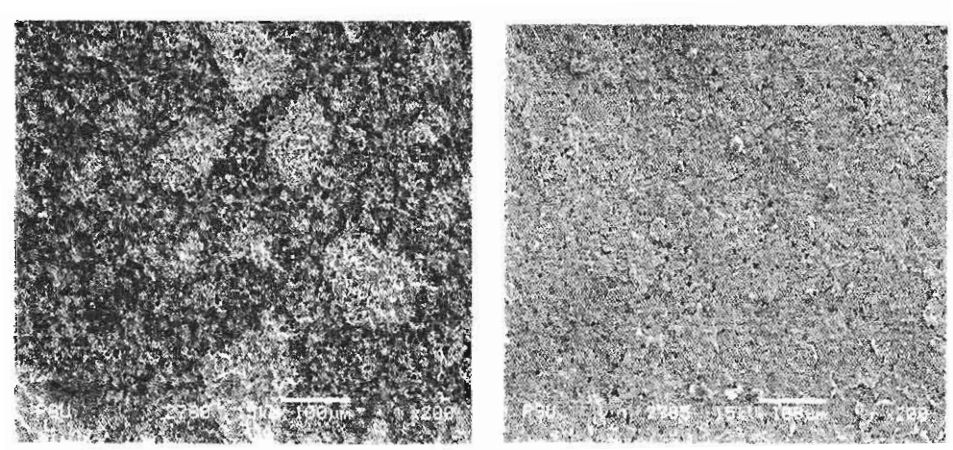

(a)

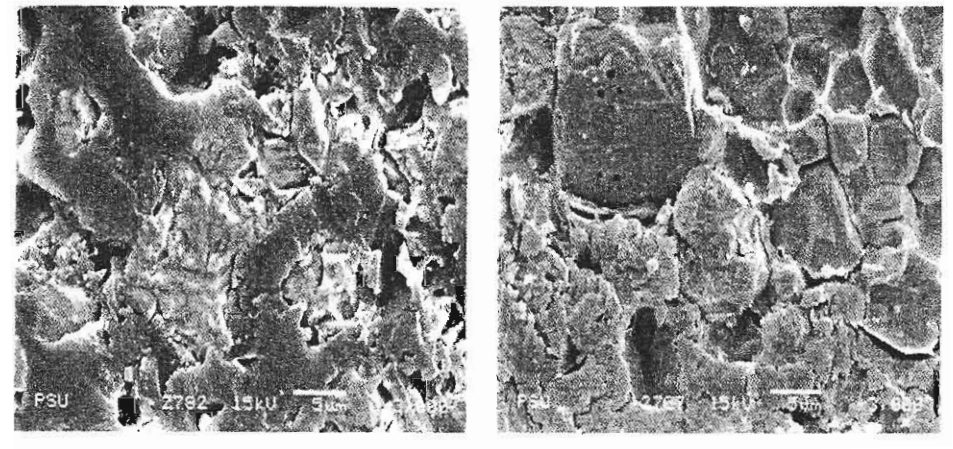

(b)

Figure 1. SEM micrographs of polished (left) and polished-etched (right) surface of PT-epoxy at (a) ×200 and (b) ×3000.

The composite samples were electroded with silver paint and subjected to a ferroelectric hysteresis measurement at room temperature and the coercive field E_c of 4.5 MV/m was observed. The samples were poled with a DC electric field of 6 MV/m for 30 min at room temperature.

Experimental Procedure

A single-beam interferometer of a Michelson type as developed by the PennState group [3] has been successfully used for determining the d_{33} piezoelectric coefficient of the 1–3 PZT-epoxy composites [4]. A similar technique was used to find a value for the poled PT-epoxy composite.

The pyroelectric coefficient was measured by detecting the charges generated for a known temperature change [5]. To minimize the humidity in the surrounding environment and avoid the softening temperature of the polymer, the measurements were made below room temperature and at a reduced pressure of 10^{-3} Pa.

Thermal diffusivity measurements [6] were made on the composite using a commercial $LiTaO_3$ wafer as a pyroelectric detector. A sinusoidally modulated laser beam from a Lasiris diode laser (Edmund Scientific Co.) was incident on the sample surface so that the heat diffused through the sample to the $LiTaO_3$ detector. The heat capacity of the sample was measured using a Differential Scanning Calorimeter (Perkin Elmer, DSC7). The unknown thermal diffusivity of the composite was analysed from the dimensions, density, heat capacity and the measured phase lag vs modulation frequency. Similar measurements were made on a glass sample with the PT-epoxy composite acting as a detector in order to determine the thermal diffusivity of the glass.

In the responsivity measurements, the modulated laser beam was incident on the electroded surface of a free-standing sample of the composite. The pyroelectric voltage was measured at different modulation frequencies. The voltage responsivity, R_V, was the voltage divided by the absorbed laser power. The voltage (F_V), current (F_I) and noise (F_D) figures-of-merit and the specific detectivity (D^*) of the composite were calculated at the frequency of the maximum responsivity of the composite. The following equations were used in the

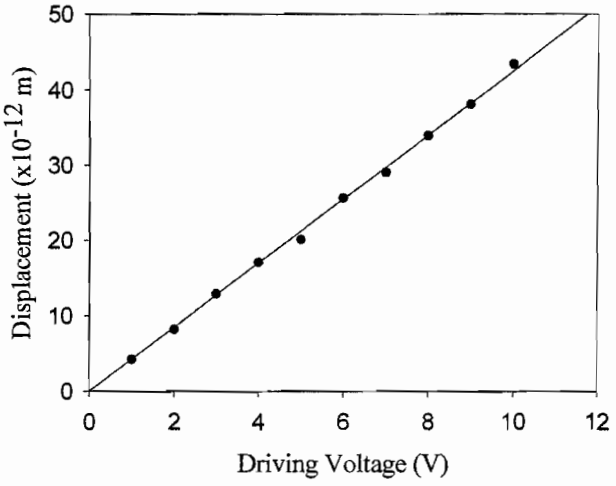

Figure 2. Piezoelectric responses at 1 kHz for 1 mm-PT-epoxy composite.

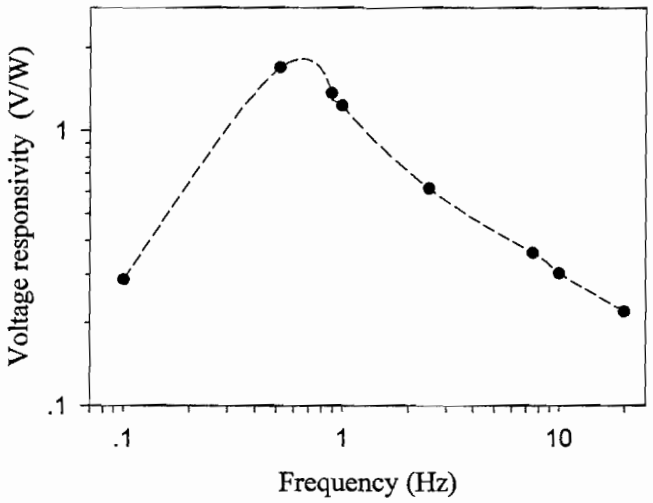

Figure 3. The voltage responsivity as a function of modulation frequency obtained from the PT-epoxy composite acting as an IR detector.

calculations [7]:

$$R_V(\max) = \eta p A[R_G/G_T(\tau_E + \tau_T)] \quad (1)$$

$$F_V = p/c'\varepsilon_r\varepsilon_0 \quad (2)$$

$$F_I = p/c' \quad (3)$$

$$F_D = p/c'(\varepsilon_r\varepsilon_0 \tan\delta)^{1/2} \quad (4)$$

$$D^* = A^{1/2}/NEP \quad (5)$$

The composite element had an area A, emissivity η, pyroelectric coefficient p, and volumetric heat capacity c'. G_T is the thermal conductance to the surroundings which gave the thermal time constant τ_T. R_G is the input resistance of the lock-in amplifier, giving the electrical time constant τ_E. τ_r and $\tan\delta$ are the relative permittivity and loss tangent of the composite, respectively. ε_0 is the permittivity of free space. NEP is the noise-equivalent power which depends upon the Johnson noise voltage and R_V.

Results and Discussions

During the interferometric measurements, the composite was rigidly glued on the substrate and only a surface of the composite was monitored. The measured d_{33} value was corrected

Table 1
Measured physical properties of PT-epoxy composite

Volume fract.	Density (10^3 kg/m^3)	Heat Capacity (J/kg °C)	Dielectric const.	$\tan\delta$	Thermal diffusivity (10^{-7} m^2/s)
50–50	4.4	200	96	0.03	2.2

Table 2
Detector properties of PT-epoxy composite compared with those of other materials

Parameter	PT-Epoxy	50/50 P(VDF/TrFE) [9]	PT [10]	PZT [11]	$LiTaO_3$ [11]
d_{33} (10^{-12} m/V)	6.0	25	56	374	9.2
p ($\mu C/m^2$ °C)	23	40	250	380	180
Fv (m^2/C)	0.031	0.11	0.046	0.059	0.14
FI (10^{-12} m/V)	26	17	78	152	56
FD (10^{-6} $m/Pa^{-1/2}$)	5.2	7.4	25	55	39
D* (10^6 $cmHz^{1/2}/W$)	1.4	—	—	—	—

for substrate clamping [8] and the value obtained was $(6.0 \pm 1.0) \times 10^{-12}$ m/V. Figure 2 shows a linear piezoelectric response observed from the PT-epoxy composite.

The pyroelectric coefficient of the composite was found to be 23 $\mu C/m^2$ °C. The low piezoelectric and pyroelectric activities were due both to incomplete poling and to porosity in the composite. At 1 kHz and room temperature the composite had a high dielectric constant of 96 and low loss tangent of 0.03.

Using a $LiTaO_3$ detector, the thermal diffusivity of PT-epoxy composite was found to be 2.2×10^{-7} m^2/s. A value of 5.1×10^{-8} m^2/s was found for a glass microscope slide using the PT-epoxy composite as a thermal detector.

For the IR detector data, Fig. 3 shows the R_v vs frequency curve. F_V, F_I, F_D and D* were found to be 0.031 m^2/C, 26×10^{-12} m/V, 5.2×10^{-6} $Pa^{-1/2}$ and 1.4×10^6 $cmHz^{1/2}/W$, respectively.

Summary

A first attempt to produce a piezoceramic-polymer composite was described in this work. SEM investigations showed a composite with 3–3 connectivity. Table 1 presents the measured physical properties of the composite. A comparison with other ceramic and polymeric materials is listed in Table 2. As seen from the tables, after further development, the PT-epoxy composite will have a good potential for various ferroelectric devices.

The relatively high detector parameters of the PT-epoxy composite showed that it could be used as an IR detector or a thermal detector in applications such as thermal diffusivity measurements. In order to make a real detector [12], the fabrication processing and various parameters of the composite will be optimized before the material is fabricated into its final form.

Acknowledgment

This work is gratefully supported by Thailand Research Fund (TRF).

References

1. R. E. Newnham, D. P. Skinner, and L. E. Cross, *Mater Res. Bull.* **13** (1978).
2. S. B. Lang and D. K. Das-Gupta, *Ferroelectrics Rev.* **2**, 3-4 (2000).
3. Q. M. Zhang, W. Y. Pan, and L. E. Cross, *J. Appl. Phys.* **63**, 8 (1988).

4. Y. Phermpornsagul, S. Muensit, and I. L. Guy, *IEEE Trans. Dielec. Electr. Insul.* (in press).
5. W. Y. Ng, B. Ploss, H. L. W. Chan, F. G. Shin, and C. L. Choy, *IEEE Int. Symp.* **2** (2001).
6. S. Muensit and S. B. Lang, *Ferroelectrics* **293**, 341 (2003).
7. R. W. Whatmore, *Rep. Prog. Phys.* **49** (1986).
8. D. Royer and V. Kmetik, *Electron. Lett.* **28** (1992).
9. N. Neumann, R. Kohler, R. Gottfried-Gottfried, and N. HeB, *Integr. Ferroelectr.* **11** (1995).
10. R. Takayama, Y. Tomita, K. Iijima, and I. Ueda, *Ferroelectrics* **118** (1991).
11. B. Ploss and S. Bauer, *Sens. Actuators A* 25–27 (1991).
12. http://www.boselec.com.

Available online at www.sciencedirect.com
ScienceDirect
Materials Research Bulletin 42 (2007) 1269–1277
Materials Research Bulletin
www.elsevier.com/locate/matresbu

Properties of lead zirconate–alumina 'nanocomposites'

Chompoonuch Puchmark [a], Sukanda Jiansirisomboon [a], Gobwute Rujijanagul [a,*], Timothy P. Comyn [b], Jing Yan He [b], Steven J. Milne [b]

[a] *Department of Physics, Faculty of Science, Chiang Mai University, Chiang Mai 50200, Thailand*
[b] *Institute for Materials Research, University of Leeds, Leeds LS2 9JT, UK*

Received 14 June 2006; received in revised form 9 August 2006; accepted 11 October 2006
Available online 28 November 2006

Abstract

Microstructures, Vickers hardness and dielectric properties of $PbZrO_3$ ceramics with co-additions of 0.5–5 vol% Al_2O_3 nanoparticles have been investigated. The additive inhibited grain growth, with average grain size decreasing from ~13 μm for $PbZrO_3$ to ~1 μm for the nanocomposites. The mode of fracture also changed, from predominantly inter-granular in $PbZrO_3$ to a mixed-mode of intra- and inter-granular fracture in the composite samples. Vickers hardness values increased from 2.9 GPa for $PbZrO_3$ to 4.1 GPa for the sample with 1 vol% Al_2O_3, but there was a more gradual increase for higher Al_2O_3 contents. Plots of relative permittivity versus temperature indicated subtle differences which were attributed to a chemical reaction between the additive and matrix during sintering. X-ray powder diffraction showed that lead aluminium oxides were the principal products of this reaction.

Keywords: A. Composites; B. Dielectric properties; C. X-ray diffraction; D. Mechanical properties; D. Microstructure

1. Introduction

Lead zirconate, $PbZrO_3$ (PZ), is an antiferroelectric ceramic and an end-member of the technologically important lead zirconate titanate (PZT) solid solution system. Although the electrical properties and phase transitions in these perovskite ceramics have been studied in detail over many years, their mechanical properties are less well understood. It is important from an applications viewpoint that $PbZrO_3$ and $Pb(Zr_{1-x}Ti_x)O_3$ ceramics are resistant to fracture or microcracking when subjected to large electric fields. For structural ceramics such as alumina, it has been demonstrated over a number of years that their mechanical properties can be enhanced by the incorporation of nano-scale particles into the microstructure [1–3]. The resulting materials are referred to as nanocomposites.

More recently, the nanocomposite approach has also been considered for improving the mechanical properties and reliability of some ferroelectric materials such as PZT [4–6]. Particles of silver, platinum and alumina have been demonstrated to improve the hardness and fracture strength of PZT [5–8]. The mechanisms resulting in the improved properties are uncertain. It has been proposed that the enhancement in mechanical properties is due to the nanoparticles reinforcing the grain boundaries, and the reduction in grain size. Diffusion of Al^{3+} onto the PZT lattice sites has also been suggested, which would alter surface and/or grain boundary energies, leading to smaller grain sizes

* Corresponding author. Tel.: +66 53 943376; fax: +66 53 357512.
E-mail address: rujijanagul@yahoo.com (G. Rujijanagul).

0025-5408/$ – see front matter © 2006 Elsevier Ltd. All rights reserved.
doi:10.1016/j.materresbull.2006.10.013